https://doi.org/10.5194/egusphere-2026-1414
Preprint. Discussion started: 4 May 2026

Soil hydrological modelling as a tool to scale EMI-estimations to direct measurements of soil water content distributions in an infiltration experiment

Antonio Coppola[1], Andrea Vacca[1], Gian Piero Deidda[2], Francesca Lobina[1], Alessandro Comegna[3], Stefania Da Pelo[1], Faiza Souid[3], Shawkat B.M. Hassan[3]

[1]Department of Chemical and Geological Sciences, University of Cagliari, Monserrato, 09042, Italy
[2]Department of Civil, Environmental Engineering and Architecture, University of Cagliari, Cagliari, 09123, Italy
3Department of Agricultural, Forestry, Food and Environmental Sciences, University of Basilicata, Potenza, 85100, Italy

Correspondence to: Shawkat B.M. Hassan (shawkat.hassan@unibas.it)

Abstract. This study explores the possibility of integrating electromagnetic induction, EMI, measurements with hydrological modelling to characterize soil hydraulic behaviour during an infiltration process at the transect scale. A controlled 10-hour irrigation experiment was conducted on bare sandy soil in Italy, where time-lapse apparent electrical conductivity, σ_a, readings were collected along a 24 m transect. Direct soil water content observations were obtained on soil samples at sites spaced 1 m apart and at five depths. Contextually, EMI readings were taken by a CMD Mini Explorer sensor and inverted to estimate bulk electrical conductivity, σ_b, distributions over time, which were subsequently converted to as many water content, θ, distributions through a site-specific θ–σ_b calibration relationship derived from independent TDR measurements taken in the upper 25 cm of soil during the infiltration experiment. Soil hydraulic properties (SHPs) for the two soil horizons of the soil profile were independently measured using the tension infiltrometer method (TIM). Two sets of hydrological simulations were carried out using a dynamic Richards-equation-based model, adopting either auger-measured initial water content profiles with the original SHPs, or EMI-estimated initial water content profiles with SHPs scaled by adjusting the saturated water content. Results show that the EMI-estimated water content distributions can effectively reproduce infiltration dynamics when appropriately scaling initial conditions and SHPs. Within this framework, scaling the SHPs and assigning initial conditions consistent with EMI observations enables the conversion between the high-frequency, microscopic description obtained from point-scale measurements and the low-frequency, macroscopic description provided by EMI monitoring. In the proposed approach, the hydrological model provides a physically based interpretative framework for understanding what an EMI sensor observes during infiltration experiments and allows for reconciling nonlinear temporal evolution of θ distributions as observed by point scale measurements and estimated by EMI during wetting front propagation without the need for empirical scaling relationships. The findings extend the results of Dragonetti et al. (2022), demonstrating that EMI monitoring combined with physically based modelling provides a robust framework for interpreting infiltration processes and estimating SHPs non-invasively at the field scale.

https://doi.org/10.5194/egusphere-2026-1414
Preprint. Discussion started: 4 May 2026

1 Introduction

One of the main objectives of hydrologist and soil scientists worldwide is to establish a practical method for estimating soil water content near the surface and across the root zone, as well as the water stored along the soil profile and its spatial distribution. The soil water distribution is influenced by soil management practices as well as by the complex, nonlinear dynamics governing water flow and solute transport in soils, which lead to uneven distributions of water (and dissolved solutes). Actually, knowing soil water conditions and patterns in the root zone over large areas is essential for many agro-hydrological applications, for example for managing irrigation, and in large scale hydrological processes such as groundwater recharge, infiltration and overland flow (Basile and Coppola, 2019). Given the crucial role of soil water content in land surface processes, its spatial and temporal distribution and trends must be evaluated at multiple scales so that it can serve as an effective tool for the strategic management and protection of water resources (Coppola et al., 2007; Comegna et al., 2010; Vereecken et al., 2016)

However, measuring soil water content across extensive areas is a complex challenge, and there are currently no large-scale monitoring networks capable of providing data at the high frequency, multiple depths, and fine spatial resolution required for various agricultural and hydrological applications.

Local-scale direct (thermogravimetric approach applied to soil samples) or indirect (Time Domain Reflectometry – TDR; Capacitive techniques) methods for measuring water contents are suitable for field plot monitoring (Robinson et al., 2003; Basile *et al.*, 2003, 2006; Comegna *et al.*, 2021; 2024) but they are not feasible for the watershed or regional scale, which would require many samples and/or sensors to analyse the spatial (and temporal) water content patterns over large scales.

For large-scale monitoring, non-invasive geophysical techniques are now available that may allow estimation of the soil water content distribution in soil profiles by relatively fast measurement campaigns on large areas and repeated over time (Hinnel et al., 2010; Lavouè et al., 2010; von Hebel et al., 2014; Huang et al., 2016; Coppola et al., 2016; Dragonetti et al., 2018; 2022). As an example, Electromagnetic Induction (EMI) sensors are now increasingly used to measure the apparent soil electrical conductivity, σ_a, which is a depth-weighted integrated soil profile response determined by the vertical distribution of depth-specific bulk soil electrical conductivity, σ_b, and by the sensor's depth sensitivity function. σ_b is controlled by several factors: (i) soil water content, θ, (ii) the electrical conductivity of the soil solution, σ_w, (iii) the tortuosity of the pore network, τ, and (iv) properties of the solid phase, such as bulk density, clay fraction, and mineral composition.

Because σ_a depends on σ_b, it is inherently sensitive to variations in soil water content (and salinity when salt concentrations are high and fluctuate across space and time). Thus, the EMI σ_a measurements collected during successive EMI surveys can be used to infer the temporal evolution of soil water content distribution, even at large scales.

Two main strategies have been used to deal with this problem: 1) The first is based on empirical calibration relationships relating integrated σ_a measurements to either θ or σ_b values coming from independent methods, such as direct sampling and TDR, at specific depth intervals. 2) The second strategy consists of applying inversion techniques to EMI data in order to retrieve the vertical profiles of σ_b, which may thus be converted to as many θ profiles using specific calibration relationships.

https://doi.org/10.5194/egusphere-2026-1414
Preprint. Discussion started: 4 May 2026

In this second case, in soils characterized by low and relatively constant salinity, a simple linear correlation between θ and σ_b may be easily obtained, based on simultaneous measurements of θ and σ_b in the field or laboratory, and reliably used to convert EMI measurements (Altdorff et al., 2018; Badewa et al., 2018; Brevik et al., 2006; Huang et al., 2016; Serrano et al., 2013). Only when salt concentrations are high and fluctuate across space and time, a single measurement of σ_b is insufficient to simultaneously estimate both θ and σ_w and a more laborious σ_b-θ-σ_w calibration relationship has to be specifically built in that case (Coppola et al., 2016; Dragonetti et al., 2022; Farzamian et al., 2021).

Within the empirical strategy, a site-specific empirical calibration can be established using various approaches, including multiple regression analysis (Triantafilis et al., 2000; Amezketa, 2006; Yao and Yang, 2010; Coppola et al., 2016), modeled coefficients (Slavich and Petterson, 1990), theoretical coefficients based on EMI depth response functions (Cook and Walker, 1992), or empirical–mathematical coefficients (Corwin and Rhoades, 1984). The first to highlight the potential of EMI sensors for detecting variations in θ were Kachanoski et al. (1988), who identified correlations between σ_a and average θ measured using TDR. Similarly, simple linear regressions were developed along a transect, linking σ_a to the total water content measured down to 1.5 m depth at different times (Sheets & Hendrickx, 1995), and across a hillslope to a depth of 0.2 m (Sherlock & McDonnell, 2003). More recently, Coppola et al. (2016) obtained depth-specific calibration relationships among multi-height EMI σ_a readings and σ_b readings coming from TDR sensors at different depths. Hedley et al. (2013) and Stanley et al. (2014) showed that ECa measurements can effectively track soil water content dynamics and are generally linearly related to independent moisture measurements.

All these empirical approaches, though apparently simple, share problems related to the site-specific characteristics of the calibration, which also change over time as soil water conditions vary, thus requiring a different calibration each time.

This is why, due also to the advances in geophysics sensors (single frequency multi-coil sensors, for example) and the increasing availability of very advanced nonlinear forward modelling developed in the last decades (Monteiro-Santos, 2004; Deidda et al., 2003; 2014; Lavoué et al., 2010; Triantafilis et al., 2013; von Hebel et al., 2014), EMI inversion approaches have become widespread in the investigation of water content and salinity in soil, allowing estimation of vertical σ_b profiles starting from the integrated σ_a readings. Single frequency multi-coil sensors are especially effective and practical for accurate reconstruction of vertical conductivity profiles from σ_a data. This is because each coil setup investigates a different, partially overlapping soil volume and, thus, provides a different σ_a reading for the same profile due to the different sensitivity function of the sensor at different coil configurations. As an example, the well-known CMD Mini-Explorer EMI sensor (GF Instruments, Czech Republic) may take σ_a measurements over six different depth sensitivity ranges. Using more σ_a readings in an inversion procedure for the same profile enhances inversion reliability. Of course, this can also be obtained by using multiple sensors simultaneously or by collecting measurements with a single sensor at different heights above the ground, but a multi-coil sensor is far more practical.

Unfortunately, when inverting the EMI σ_a data to obtain σ_b profiles, one invariably finds discrepancies, at various degree, between EMI-based σ_b spatial distributions and those coming from local scale direct sampling or TDR measurements (Coppola

https://doi.org/10.5194/egusphere-2026-1414
Preprint. Discussion started: 4 May 2026

et al., 2016; Dragonetti et al., 2018; 2022; Farzamian et al., 2021; Autovino et al., 2026) or other geophysical approaches, such as Electrical Resistivity Tomography (ERT) (Von Habel et al., 2014). These differences have been attributed to different reasons, related to the sensor electronic or to the observation volume.

Firstly, frequency-domain EMI measurements, like all physical observations, are inherently influenced by noise. Systematic variations in apparent conductivity may also arise from instrumental drift, calibration inaccuracies, or environmental factors, including temperature fluctuations, solar radiation, power supply instability, operator proximity, zeroing procedures, nearby conductive objects, or specific field deployment conditions. All issues that cannot be fully identified and systematically corrected. Consequently, the reliable interpretation of σ_a data requires comprehensive and well-structured calibration procedures (von Habel et al., 2014).

However, apart from the drift issues inherent in the EMI measurements, many papers in the literature have discussed the dominant role of the different observation volume of EMI sensors and that of the local scale observations coming for TDR or direct sampling (Coppola et al., 2016; Dragonetti et al., 2018; 2022; Farzamian et al., 2021; Autovino et al., 2026). The observation volume of an EMI sensor for soil studies is approximately $10^5 – 10^6$ cm³, whereas a typical soil core has a volume of 100–150 cm³ and a TDR probe explores a volume of ~10^3 cm³. Due to their relatively small observation volume, soil samples or TDR sensors provide quasi-point measurements and are therefore more effective at capturing small-scale variability in soil quantities, such as water content and solute concentrations, arising from natural heterogeneity. Consequently, variability within a set of samples or TDR readings reflects both small- and large-scale heterogeneities, corresponding to high- and low-spatial-frequency components. In contrast, EMI measurements, owing to the instrument size and underlying physical principles, inherently integrate over small-scale variability observed at the TDR scale. It is thus obvious that one cannot expect perfect matching at point scale. In a correct approach, one should first upscale sample measurements or TDR estimations to EMI support volume before comparison. In this direction, Coppola et al. (2016) and Dragonetti et al. (2018) applied a low-pass filter based on the Fourier transform to the point-scale TDR series, effectively removing high-spatial-frequency components and making the TDR data comparable with EMI measurements.

Another issue is related to the reliability of the inversion of the EMI σ_a data. Converting profile-integrated EMI measurements into a vertical distribution σ_b is an ill-posed problem, characterized by non-uniqueness, i.e., multiple possible solutions and instability. Small data errors or incomplete information can cause large variations in the estimated parameters (see, for example, Tarantola, 1987). Ill-posed problems are typically addressed through regularization of the inverse solution. However, the choice of regularization approach and its parameters can strongly influence the outcomes (e.g., Dragonetti et al., 2018; Zare et al., 2020). In fact, it has been noted that this type of regularization may not accurately represent actual hydrologic conditions and can reduce the reliability of soil hydrological quantities and properties estimates derived from geophysical data (Hinnel et al., 2010).

https://doi.org/10.5194/egusphere-2026-1414
Preprint. Discussion started: 4 May 2026

In general, the result of the inversion process's different observation volumes and regularization is a smoother response in the electrical conductivity. The inversion partially shades thin wet layers or the sharp changes in water contents, e.g., at the propagation of a wetting front.

Some strategies were developed to calibrate EMI without inversion by using the conductivity models obtained from Electrical Resistivity Tomography, ERT, as inputs for EMI forward simulations (von Habel et al., 2014). The resulting simulated σ_a is compared to those measured by EMI to calibrate it (see figure 7 in von Habel et al., 2014). This data-space calibration, however, strongly depends on the ERT inversion accuracy, which, like EMI, is an ill-posed problem. Both EMI and ERT inversions are highly sensitive to data quality and the regularization framework. They should incorporate prior constraints like known profile discontinuities. Also, ERT measurements are time and effort consuming at large scales. Moreover, EMI data still need inversion if the goal is to obtain σ_a distributions. Therefore, model-space calibrations are more widely used, where the calibrations are carried out on the σ_b distributions coming from preliminary inversion of σ_a series (Coppola et al., 2016; Dragonetti et al., 2018; 2022; Farzamian et al., 2021; Autovino et al., 2026) rather than on the original σ_a series themselves.

All the efforts to make EMI readings comparable to local scale measurements remain largely empirical, sometimes speculative, without a well-identified physical basis explaining the different distributions of soil water content, θ, or σ_b obtained from the two measurement types. Additionally, calibration relationships are site-specific and vary over time and depth due to non-linear hydrological processes and the non-linear EMI response during infiltration and redistribution.

From this perspective, soil hydrologic modelling may provide a physically based interpretation of what geophysical measurements are looking at. Indeed, numerical simulations of the same hydrological processes monitored by an EMI sensor can provide insight into the likely direction of the EMI inversion, as they help anticipate the expected sensor response and its spatial and temporal variability (Hinnel et al., 2010; Farzamian et al., 2020).

In this direction, hydrological models may be used in different approaches for interpreting EMI data. On one side, the EMI data may be used as input data in a soil hydrological model to optimize the soil hydraulic properties of the system under study, by forcing the hydrological model to reproduce the time-lapse EMI σ_a data observed over time during a water infiltration process. Within this framework, either coupled or uncoupled approaches may be used (Camporese et al., 2015). The pros and cons of the two different approaches to identify water and/or solute propagation have been discussed, for example, in in Hinnel et al. (2010), Camporese et al. (2015) and Dragonetti et al. (2022).

In an effort to provide a physical interpretation of what is really captured by local-scale measurements and by electromagnetic induction data during time-lapse monitoring of an infiltration process, Dragonetti et al. (2022) investigated an artificial rainfall experiment conducted on a soil plot, which was interpreted through an uncoupled framework, and the reliability of the approach was assessed by comparison with TDR and tensiometer measurements. The uncoupled approach followed a three-step procedure, where the θ distributions deduced by the EMI readings were employed as measurements in an iterative procedure to estimate the soil hydraulic parameters required to simulate the wetting front dynamics during the infiltration experiment in a Richards equation-based numerical modelling framework. In parallel, the soil hydraulic properties were also obtained using the θ and pressure heads monitored in the soil profile by TDR probes and tensiometers, respectively, serving as the reference

https://doi.org/10.5194/egusphere-2026-1414
Preprint. Discussion started: 4 May 2026

measurements for estimating the hydraulic parameters. It is worth noting that, in their approach, the authors intentionally chose not to scale the original EMI σ_a nor the σ_b derived from the EMI inversion, as the aim was just to assess how the TDR direct measurements and the EMI observations captured the same infiltration process. Obviously, the two simulations differed in their initial conditions, with the TDR-derived water content and the EMI-derived water content used respectively for each case.

The inversion of the soil hydrological model under the two scenarios produced TDR- and EMI-based water retention curves simply scaled according to the ratio between the saturated water contents estimated from TDR and EMI data, whereas hydraulic conductivity curves were largely overlapping, reflecting the overall similar shape of the water retention curves. These findings indicated that the TDR measurements and EMI sensor essentially observed the same infiltration process, with differences arising only from the distinct saturated water contents and initial conditions. By adjusting the water retention curves according to the saturated water content ratio and applying sensor-specific initial conditions, the authors were able to accurately reproduce the temporal evolution of the infiltration process observed by both measurement methods, despite differences in the spatial distributions of water content measured by TDR and EMI.

To us, this seems an interesting interpretative key and has important implications for understanding what an EMI sensor and local-scale measurements can actually observe in a hydrological process, such as the propagation of a wetting front during infiltration. Indeed, if the results above were confirmed, there would be no need to empirically scale the EMI measurements to match point-scale data. Instead, the hydrological model itself could provide a consistent framework to reconcile the two seemingly different observations from TDR and EMI by appropriately scaling the initial water contents observed by the two techniques and the saturated water contents of their respective water retention curves. In other words, the model itself would provide the scaling tool to directly reconcile the two seemingly different hydrological processes, rather than empirically adjusting the σ_b or θ time series observed by the local-scale techniques and the EMI at each time and depth.

The findings in Dragonetti et al. (2022), however, are based on a limited experiment conducted on a silty loam soil over a relatively small plot. Further validation through larger-scale experiments and across different soil types is required. In this context, the present study examines an experiment performed at the transect scale, extending the analysis to a broader spatial domain and a different soil type. Therefore, this paper aims at extending the findings of Dragonetti et al. (2022) by using the FLOWS physically-based agrohydrological model to understand what EMI sensor observes, in terms of water contents and the soil hydraulic properties, in sandy soils at transect scale. The paper also aims at comparing between the spatio-temporal distributions of the water contents calculated by the agrohydrological model using the initial conditions obtained by auger sampling and those estimated by EMI. Another objective of this study is to scale the EMI-estimated initial conditions to those obtained by auger samples and use the scaled initial conditions in the agrohydrological model to analyse the resulting simulated water content spatio-temporal evolution.

https://doi.org/10.5194/egusphere-2026-1414
Preprint. Discussion started: 4 May 2026

The paper is based on time-lapse EMI σ_a measurements collected along a 24 m transect during a controlled 10-hour irrigation experiment conducted on a bare sandy soil in Italy. The propagation of the wetting front was monitored using continuous EMI and simultaneous water content measurements at sites spaced 1 m apart and at five different depths, which were used as a sort of replicated soil profile observations. Both measurement series were also simulated using independently measured soil hydraulic properties for the two layers identified in the soil profile. The simulations were performed using initial water content conditions obtained respectively from direct sampling and EMI, with the main aim of validating, extending and generalizing the results of Dragonetti et al. (2022), with a view to a more applicative scale transferability of the approach.

2 Materials and Methods

2.1 The experimental transect

The study site is located in Arborea Plain in the province of Oristano, Sardinia Island, Italy (Geographic coordinates: 39° 45' 54.47" N, 8° 34' 37.92" E) as shown in Figure 1. Arborea area is a hydraulically reclaimed area and is utilized in intensive livestock activities. This is why it is mostly cultivated by fodders, in particular, corn and ryegrass.

The investigated soil profile is mostly sandy (even more than 90% sand) and consist of two main horizons: the first, more structured, from 0 to 30 cm containing organic matter coming from manure fertilization (A horizon); the second one, from 30 to the groundwater, very loose (C horizon). The soil has been classified as Arenosol (IUSS Working Group WRB, 2022).

https://doi.org/10.5194/egusphere-2026-1414
Preprint. Discussion started: 4 May 2026

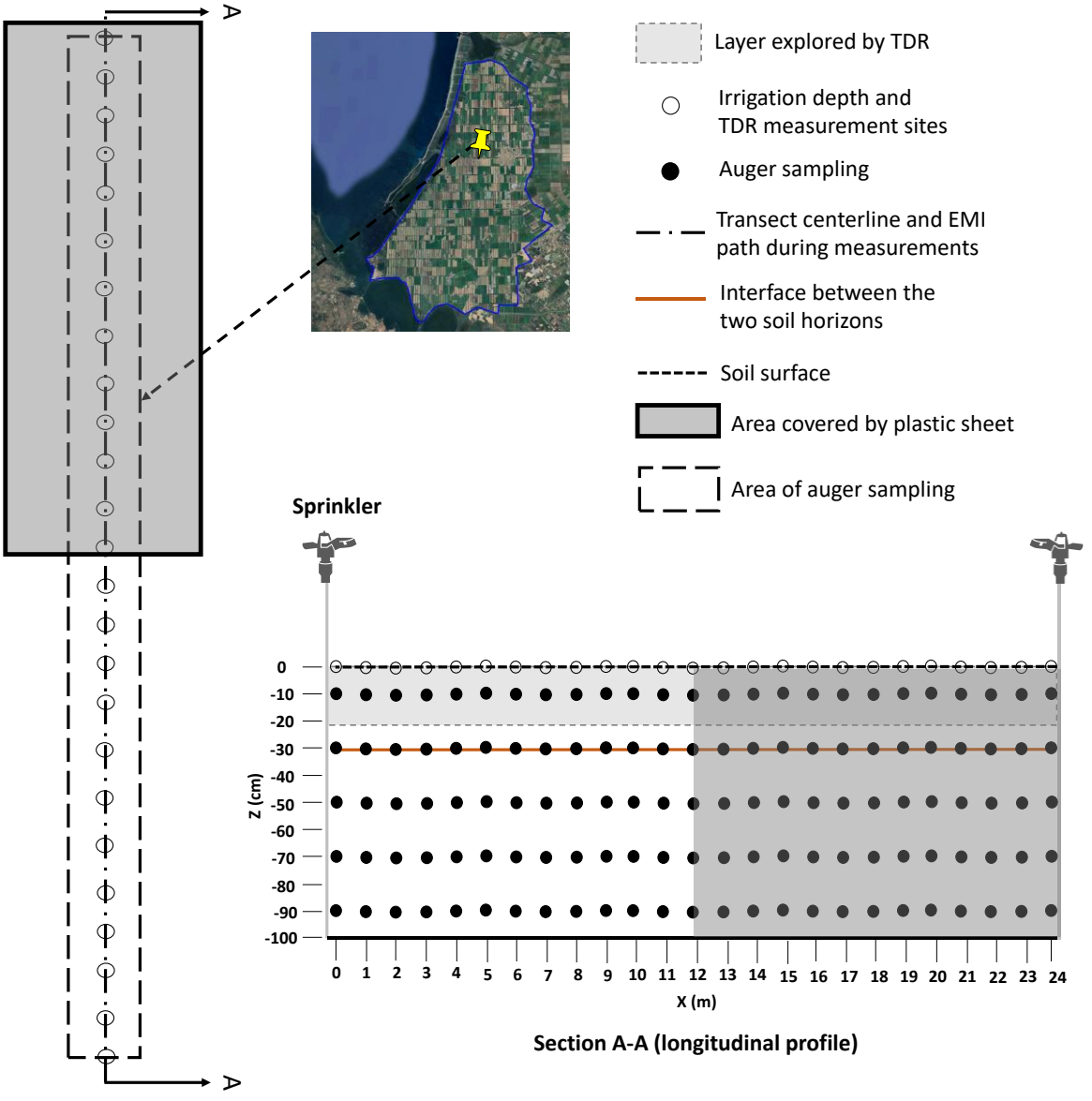

Figure 1: Schematic view (not to scale) of the experimental transect, along with a vertical section showing the sampling and measurement positions. The open circles at the soil surface represent measurement sites at 1-meter distances that were used for TDR measurements at the soil surface, as well as for irrigation uniformity assessment. These measurement points were numbered consecutively from 0 to 24; The dashed centerline indicates the path for continuous EMI measurements; The solid circles indicate auger sampling, which was carried out at five different depths. The auger sampling at different times was taken along different lines lying in the band indicated by the dashed rectangle (about 1.3 m width); The shadowed area in the vertical section was only sampled for the initial characterization, even if EMI measurements were still performed during the second monitoring day. The details are given in the text. The map at the top shows the Arborea Plain (blue borders) on top of a Google satellite image of the area (Imagery ©2026 Airbus, CNES / Airbus, Maxar Technologies, Map data ©2026).

https://doi.org/10.5194/egusphere-2026-1414
Preprint. Discussion started: 4 May 2026

The experiment was carried out along a 24 m x 1.3 m transect, which covers the distance between two sprinklers, as shown in Figure 1. A sprinkler applies irrigation at a nominal rate of 10 l/s on a range of 10 m. A piezometer installed close to the transect was used to monitor the depth to groundwater, which was at about 120 cm at the beginning of the experiment. The experiment took place on May 13th and 14th, 2024, when the soil was relatively dry and there was no crop cultivated. It lasted about 10 hours and consisted of an infiltration process induced by a controlled rainfall coming from sprinklers, which was monitored by direct soil sampling, as well as by TDR and EMI measurements (see the Figure 1). The first day was devoted to defining the initial water content conditions of the soil profile, whereas the infiltration test was carried out during the second day. During this second day, half of the transect was covered with waterproof plastic sheet, to serve as a reference for evaluating the goodness of EMI inversion in the irrigated half-transect.

Thus, the sprinkler irrigation was activated five times, each time lasting one hour. After each hour of sprinkler irrigation, irrigation stopped for one hour to carry out a round of measurements. Therefore, a total of six rounds of measurements were taken. Table 1 summarizes the experiment's timeline and the measurements taken during each round.

Table 1. A timeline of the rounds of measurements taken during the experiment

Day	Time	Irrigation	Measurements
May 13th, 2024	*Initial conditions* ($t = 0$)	Off	– TDR surface measurements – Auger samples – EMI measurements along the transect
May 14th, 2024	$t = 0 – 1$ h	On	– Cylinders for irrigation depth
	$t = 1 – 2$ h	Off	– TDR surface measurements – Auger samples – EMI measurements along the transect
	$t = 2 – 3$ h	On	No measurements
	$t = 3 – 4$ h	Off	– TDR surface measurements – EMI measurements along the transect
	$t = 4 – 5$ h	On	– Cylinders for irrigation depth
	$t = 5 – 6$ h	Off	– TDR surface measurements – Auger samples – Cylinders for irrigation depth – EMI measurements along the transect
	$t = 6 – 7$ h	On	No measurements
	$t = 7 – 8$ h	Off	– TDR surface measurements – EMI measurements along the transect
	$t = 8 – 9$ h	On	– Cylinders for irrigation depth
	$t = 9 – 10$ h	Off	– TDR surface measurements – Auger samples

https://doi.org/10.5194/egusphere-2026-1414
Preprint. Discussion started: 4 May 2026

			- EMI measurements along the transect

Several measurements were taken along the transect at each monitoring round, included the characterization of the initial condition: 1) TDR measurements at the soil surface. Two different probes were used, both inserted vertically at the soil surface, with a length of 15 cm and 25 cm, respectively; 2) Disturbed auger samples, taken at 1 m distance and at five different depth intervals: 0 – 20, 20 – 40, 40 – 60, 60 – 80, 80 – 100 cm. 3) EMI measurements acquired, in a continuous mode, by using a CMD Mini explorer sensor.

For the characterization of the initial conditions, TDR measurements and auger sampling were carried out along the entire transect. On the second day, these measurements were conducted only along the irrigated half of the transect (twelve sites), whereas EMI measurements were still performed along the entire transect. Three times during the experiment, the irrigation depth was sampled by cylinders to characterize the irrigation uniformity along the transect.

2.2 Building of the site-specific σ_b-θ relationship

As known, TDR measurement technique allows for measuring simultaneously both θ and σ_b in the same observation volume (Heimovaara et al., 1995; Robinson et al., 2003, among others). The device used in this study was TDR200 (Campbell Scientific, Logan, UT, USA). The TDR200 device releases an electromagnetic pulse into a coaxial system including the probe. The wave is then reflected, and the reflectometer samples the reflected wave. The reflected wave is then analysed by the software PC-TDR (Campbell Scientific, Utah, USA).

For each monitoring time, immediately after the EMI survey, direct measurements of θ and σ_b were collected in the surface soil horizon (0–30 cm). A TDR probe was inserted vertically at the soil surface at each monitoring site. Two different three-rod probes were used, to have two observation volumes each time at each site, one of 15 cm length and 5 cm outer rod spacing, the other of 25 cm length and 10 cm outer rod spacing. Both the probes were connected to a 200-cm-long RG58 antenna cable (50 Ω characteristic impedance and 0.2 Ω connector impedance)

The apparent dielectric constant of the soil, Ka, was derived from the propagation velocity, v, of the electromagnetic wave traveling through the soil:

$$K_a = \left(\frac{c}{v}\right)^2 \quad (1)$$

where c is the velocity of electromagnetic waves in free space, and v is calculated from the time interval between the arrival of the two reflected signals, accounting for the round-trip travel length of the probe, as recorded by the sampling oscilloscope of the cable tester.

Soil water content, θ, was then estimated from K_a using the empirical relationship proposed by Topp et al. (1980):

https://doi.org/10.5194/egusphere-2026-1414
Preprint. Discussion started: 4 May 2026

$$\theta = -5.3 \times 10^{-2} + 2.92 \times 10^{-2} K_a - 5.5 \times 10^{-4} K_a^2 + 4.3 \times 10^{-6} K_a^3 \quad (2)$$

The Tektronix 1502C measures the total resistance (R_t) of the transmission line as:

$$R_t = Z_c \left[\frac{1+\rho\infty}{1+\rho\infty}\right] = R_s + R_c \quad (3)$$

where R_s represents the soil contribution to the total resistance, R_c accounts for the series resistance of the cable and connector, Z_c is the characteristic impedance of the transmission line, and ρ∞ is the reflection coefficient at long times, once the waveform has stabilized.

The bulk electrical conductivity normalized to 25°C ($\sigma_{b,25°C}$) was calculated according to Rhoades and van Schilfgaarde (1976) and Wraith et al. (1993):

$$\sigma_{b,25°C} = \frac{f_c}{R_s} . f_T \quad (4)$$

where f_c is the cell constant of the TDR probe and f_T is a temperature correction factor applied when measurements are taken at temperatures other than 25°C. Both R_c and f_c were determined by measuring R_t with the TDR probe immersed in a solution of known electrical conductivity.

Each of the two TDR probes was not permanently installed within the soil surface in order to avoid interference between the metallic TDR rods and the EMI measurements.

All the TDR-based θ and σb data taken during all the infiltration test duration were used to build an independent soil-specific calibration relationship to be used for converting the σ_b coming from the EMI inversion to as many θ values.

2.3 Auger samples analysis

As said, disturbed soil samples were collected from the surface down to a depth of 90 cm at 1 m intervals along the transect and at five different depths. Due to the destructive nature of the sampling procedure, subsequent auger sampling lines were positioned within 0.25 m of one another along the transect. These samples were sealed in a bag and transported to the laboratory for the gravimetric water content, θ_g, measurement. In addition, five undisturbed samples were collected at an excavation pit from the five depth intervals (e.g., every 0.2 m). The undisturbed samples were then used to obtain the dry bulk densities, ρ_b, of the different depth intervals, and thus the volumetric water content, θ, from θ_g, as well as to determine the saturated water content, θ_s.

2.4 Inversion of EMI σ_a data

The propagation of the wetting front during the irrigation was tracked using a CMD mini-explorer EMI sensor (GF Instruments, Brno, Czech Republic). Measurements started immediately after the irrigation stop. They were first taken in vertical coplanar

https://doi.org/10.5194/egusphere-2026-1414
Preprint. Discussion started: 4 May 2026

(VCP; horizontal magnetic dipole) mode and then in horizontal coplanar (HCP; vertical magnetic dipole) mode by rotating the probe of 90°. The sensor operates at 30 kHz and features three receiver coils located 0.32, 0.71, and 1.18 m from the transmitter coil, referred to as "ρ32," "ρ71," and "ρ118." As a result, six different σ_a values were obtained (three coil offsets × two orientations), each corresponding to a specific depth sensitivity.

Time-lapse ρ_a measurements acquired during the experiments were inverted to obtain ρ_b distributions in time. The inversion relied on the algorithm introduced in Deidda et al. (2014) and later extended in Deidda et al. (2020) to process both the in-phase and quadrature components of the instrument's complex response, as well as to incorporate a regularization term encouraging sparse solutions.

The forward modelling used to compute the nonlinear electromagnetic response of a layered half-space excited by a dipole source is well established (Hendrickx et al., 2002; Wait, 1982; Ward and Hohmann, 1988). Thanks to the cylindrical symmetry of the system, the magnetic field detected by the receiver is independent of rotations of the tool around its vertical axis. Model predictions, expressed as the ratio between secondary (HS) and primary (HP) magnetic fields for both HCP and VCP coil configurations, are given by:

$$\begin{cases} M^{HCP}(\boldsymbol{\sigma},\boldsymbol{\mu};h,\omega,\rho) = -\rho^3 \int_0^\infty e^{-2\lambda h}\lambda^2 R_{\omega,0}(\lambda) J_0(\rho\lambda) d\lambda \\ M^{VCP}(\boldsymbol{\sigma},\boldsymbol{\mu};h,\omega,\rho) = -\rho^2 \int_0^\infty e^{-2\lambda h}\lambda R_{\omega,0}(\lambda) J_1(\rho\lambda) d\lambda \end{cases} \quad (5)$$

where $\boldsymbol{\sigma}$ and $\boldsymbol{\mu}$ represent the conductivity and the magnetic permeability vectors related to soil layers, λ is an integration variable representing the depth below the ground, normalized by the inter-coil distance r, J_0 and J_1 are Bessel functions of the first kind of zeroth and first orders, respectively, and $R_{\omega,0}(\lambda)$ is the response kernel. The kernel $R_{\omega,0}(\lambda)$, which is a complex value function of the parameters that describe the layered subsurface (conductivity, magnetic permeability, and layer thickness) besides the frequency and λ, can be written as:

$$R_{\omega,0}(\lambda) = \frac{N_0(\lambda) - Y_1(\lambda)}{N_0(\lambda) + Y_1(\lambda)} \quad (6)$$

where $Y_1(\lambda)$ and $N_0(\lambda) = \lambda/(i\omega\mu_0)$ are the surface admittance and the intrinsic admittance of the free space, respectively; in the latter, i is the imaginary unit, ω is the angular frequency, and μ_0 is the magnetic permeability of the free space. Setting $Y_n(\lambda) = N_n(\lambda)$, $Y_1(\lambda)$ can be obtained using Wait's back-recursive formula:

$$Y_k = N_k \frac{Y_{k+1} + N_k \tanh(d_k u_k)}{N_k + Y_{k+1}\tanh(d_k u_k)}, \; k = n-1,\ldots,1 \quad (7)$$

where d_k represents the kth layer thickness and

$$N_k = \frac{u_k(\lambda)}{i\omega\mu_k} \quad (8)$$

https://doi.org/10.5194/egusphere-2026-1414
Preprint. Discussion started: 4 May 2026

is the intrinsic admittance of the *k*th layer, with

$$u_k(\lambda) = \sqrt{\lambda^2 + i\sigma_k\mu_k\omega}N_k = \frac{u_k(\lambda)}{i\omega\mu_k} \quad (9)$$

If the objective of the survey is to reconstruct the vertical profile of electrical conductivity σ_k (k = 1, …, M) from electromagnetic measurements collected at n coil spacings (such as those provided by the CMD mini-explorer), the best approximation $\hat{\boldsymbol{\sigma}}$ can be found minimizing the Euclidean norm of the complex residual vector $\mathbf{r}(\boldsymbol{\sigma})$ between the complex data $\mathbf{b}(r_i)$ (i = 1, …, n) and the complex model prediction $M(\boldsymbol{\sigma})$, that is,

$$\hat{\boldsymbol{\sigma}} = arg \min_{\boldsymbol{\sigma}\in\mathbb{R}^M} \frac{1}{2}\|\mathbf{r}(\boldsymbol{\sigma})\|^2 \quad (10)$$

The nonlinear optimization problem is solved through a damped and regularized Gauss-Newton scheme, described in detail by Deidda et al. (2023). At each iteration, the problem is linearized using a first-order Taylor expansion. The method benefits from an exact Jacobian (Deidda et al., 2014), which increases both speed and accuracy compared to finite-difference approximations. The damping factor is chosen to guarantee convergence and to maintain physically meaningful (positive) conductivity values. Each linear subproblem is stabilized using truncated generalized singular value decomposition (TGSVD; Díaz de Alba and Rodriguez, 2016) with multiple options for regularization. Alongside classical first- and second-derivative operators, we also tested a nonlinear stabilizer designed to emphasize block-like features (Zhdanov et al., 2006; Ley-Cooper et al. 2015; Vignoli et al. 2015; Vignoli et al. 2017). This more recent regularization approach can reduce the over-smoothing common in traditional inversions, particularly when sharp contrasts are expected, and thereby enhance the subsequent calibration of EMI-derived results against TDR measurements. For this reason, the EMI reconstructions employed in this work correspond to those obtained using this "sharp" inversion strategy.

Electromagnetic observations alone do not allow us to identify the optimal model unambiguously. In our study, we assumed that immediately after irrigation the effect of water is largely confined to the shallowest layers. Under this assumption, the sharp inversion approach produced results that appeared more realistic. Nevertheless, since the calibration process targets the EMI-inferred models rather than the original data, the final calibrated results inherently reflect the regularization choices adopted during inversion.

The reliability of the inversion strategy was also checked by examining the σ_b distributions retrieved from the area of the transect covered by a plastic sheet. The inversion was considered reliable if the σ_b pattern in the non-irrigated region remained temporally stable.

Finally, the spatiotemporal distributions of σ_b values obtained from the inversion of EMI data collected during the infiltration process were then converted into corresponding θ distributions using the site-specific ρ_b–θ relationship described above. From these distributions, twelve profiles of EMI-based θ values were resampled for each of the sampling times, to be compared to the twelve θ profiles obtained by auger sampling.

https://doi.org/10.5194/egusphere-2026-1414
Preprint. Discussion started: 4 May 2026

2.5 Soil hydraulic properties

A pit was excavated in the study area to characterize the pedological horizons, along with their textures and hydraulic properties. Two soil horizons were observed and their Soil Hydraulic Properties, SHP, were characterized using the Tension Infiltrometer Method (TIM) (Ankeny et al., 1988; Hassan et al., 2022; 2025).

Initially, the soil surface was carefully levelled. A ring was then positioned on the ground, and a thin layer of uniform fossil sand was spread over the surface to ensure proper contact with the 10-cm-radius infiltrometer disc.

At each location, infiltration tests were conducted sequentially under four water pressure head values (−15, −10, −5 and −1 cm). The applied pressure was regulated by adjusting the height of the tube in the bubble tower. Soil samples were collected both before and after infiltration to determine the initial and final water content.

Cumulative infiltration data served as input for an inverse solution of the 3D Richards equation for water flow using DISC software (Simunek and van Genuchten, 1996), allowing the estimation of the hydraulic parameters through a parameter optimization procedure. The SHP were parameterized by using the van Genuchten-Mualem model (van Genuchten, 1980; Mualem, 1976):

$$S_e = \frac{\theta-\theta_r}{\theta_s-\theta_r} = [1 + |\alpha_{VG}h|^n]^{-m} \quad (11)$$

$$K_r(S_e) = \frac{K(S_e)}{K_0} = S_e^{\tau}\left[1-\left(1-S_e{}^{1/m}\right)^m\right]^2 \quad (12)$$

In the equations above, S_e is the effective water saturation, θ_s is the saturated water content, θ_r is the residual water content, and β, n, and m are fitting parameters, with m=1-1/n. Finally, K_s is the saturated hydraulic conductivity, and τ is the pore-connectivity parameter. The parameters for the two horizons considered in this paper are summarised in the **Table 2**. As shown in the table, the residual water content was assumed to be zero because the soil is sandy, which typically displays low negligible residual water content values (Schaap and Bouten, 1996).

Table 2. The soil hydraulic parameters of the two soil horizons in the study site

Horizon	Depth (cm)	ρ_b (g/cm^3)	θ_s	θ_r	α_{VG} (cm^{-1})	n_{VG}	K_s (cm/h)	τ
1	30	1.90	0.270	0	0.064	1.220	12.500	0.5
2	100	1.80	0.302	0	0.060	1.200	2.083	0.5

2.6 Soil hydrological simulations

Richards' equation-based soil hydrological simulations were carried out to describe the propagation of the wetting front during the infiltration experiment along the transect. Since the soil is very sandy, lateral fluxes, potentially induced by horizontal variability in soil hydraulic properties or by spatially variable rainfall at the surface, are expected to be negligible. On one side, this assumption implies that each of the twelve θ profiles coming from the auger sampling is mostly independent on the

https://doi.org/10.5194/egusphere-2026-1414
Preprint. Discussion started: 4 May 2026

surrounding ones. Related to this, the assumption also justifies the use of a 1D soil hydrological modelling approach to describe the water flow in each of the twelve sampling sites.

The physically based model FLOWS (Coppola et al., 2025) was used for these 1D simulations. FLOWS is a dynamic model simulating water flow and solute transport within the soil–plant–atmosphere system by numerically solving the one-dimensional Richards equation for water movement and the one-dimensional advection–dispersion equation. It has been previously presented in several studies (Coppola et al., 2019, 2024; Fusco et al., 2024; Hassan et al., 2024; Porru et al., 2024; 2026a, b) and is now incorporated into a client–server architecture that allows users to interact directly with the model through a web browser (https://flows.unica.it/).

FLOWS requires specifying the top boundary, bottom boundary and initial conditions, as well as the SHP for the soil horizons to be simulated. We assumed that SHPs obtained by infiltrometer characterization of each of the two soil horizons identified apply for all the 1D soil profiles considered, by thus neglecting their possible variability along the transect. The top boundary conditions were set as variable fluxes corresponding to the measured irrigation depths using the cylinders. The bottom boundary conditions were set as variable soil water pressure head equal to the difference between the profile depth and the measured depth to groundwater table. The bottom boundary pressure head was considered positive when the groundwater table was above the bottom of the flow field, and negative when below the bottom of the flow field. The initial conditions were set as the measured water contents at different depths, in the case of the auger, and at the estimated water contents at the same depths, in the case of EMI. Appropriately setting the initial conditions is a very important issue in the context of this paper, as will be discussed later in the results, because of the short simulation duration, during which the influence of the initial soil water distribution remains significant.

For each of the twelve sites, the simulated θ profiles were compared to each of the simulated soil profiles. Specifically, the simulated θ profiles to be compared to the observed θ profiles coming from the auger soil samples were obtained by using the original SHPs obtained by the infiltrometer method. By contrast, the simulated θ profiles to be compared to the estimated θ profiles coming from EMI were obtained by simply scaling the saturated water content of the water retention curves, as suggested by Dragonetti et al. (2022).

The simulation domain extended to a depth of 100 cm, with two different soil layers (0-30 cm and 30-100cm), and was discretised in 100 simulation nodes.

2.7 A summary of the hydro-geophysical approach

Overall, twenty-four FLOWS simulations were performed. Twelve simulations used the auger-measured water contents as initial conditions together with the original SHPs for the two soil horizons. The remaining twelve simulations used the EMI-estimated water contents as initial conditions and water retention curves scaled through a saturated water content scaling factor. In the second case, different scaling factors were tested in order to achieve the best agreement between the simulated and EMI-estimated θ profiles.

https://doi.org/10.5194/egusphere-2026-1414
Preprint. Discussion started: 4 May 2026

Figure 2 provides a schematic view of the approach followed in the paper. First, SHP were measured using TIM for the two identified soil horizons. Then, throughout the experiment, TDR surface measurements were carried out, at the initial conditions and after each irrigation, to calibrate a θ-σ_b relationship and to obtain a top-boundary condition for the time-lapse inversion of EMI data. Time-lapse inversions of σ_a measured by EMI at different depths led to the estimation of spatio-temporal distribution of σ_b, which in turn was converted to θ using the calibrated θ-σ_b relationship obtained by TDR data.

Auger samples were collected at five different depths at each of the twelve sites to obtain baseline θ data. Thus, two distributions of θ values were obtained: one is directly measured by auger sampling, and the other is estimated by EMI.

Using the SHP measured by TIM, two sets of FLOWS simulations were conducted: one using the EMI-estimated θ data as initial conditions and the other using the auger-measured θ data as initial conditions. The auger-measured θ values were compared to those simulated by FLOWS using auger-measured initial conditions. Similarly, the EMI-estimated θ values were compared to those simulated by FLOWS using EMI-estimated initial conditions. Then, the initial conditions estimated by EMI were scaled to those obtained by auger. This scaling was done by multiplying the EMI-estimated initial conditions by a scaling factor which was variable by depth, so that, at each depth, the average EMI-estimated initial water contents were equal to the average auger-measured initial water contents. Then, the new scaled initial conditions were used to carry out new FLOWS simulations whose results were compared to those carried out using auger-measured initial conditions.

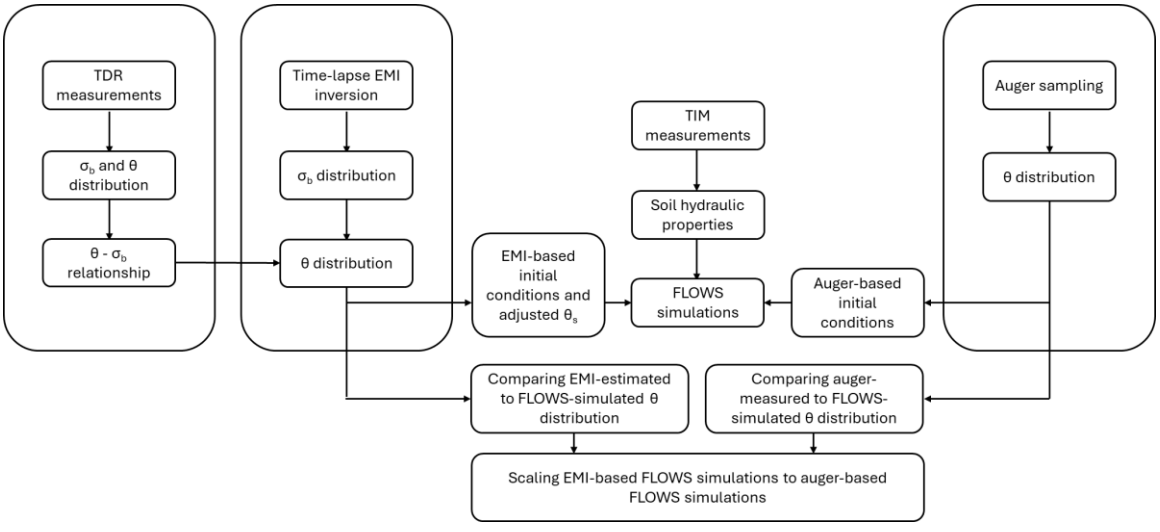

Figure 2: Schematic view of the hydro-geophysical approach followed in this paper. An explanation is provided in the text.

https://doi.org/10.5194/egusphere-2026-1414
Preprint. Discussion started: 4 May 2026

3 Results and discussion

3.1 Obtaining σ_b distributions from the inversion of the EMI σ_a readings

Figure 3 shows the spatial distribution of the EMI σ_a under the VCP configuration and HCP configuration for the three receiver coil spacings (ρ32, ρ71, and ρ118) measured at the beginning (t=0) and during the water infiltration experiment after the 3h (after 2nd irrigation), 5h (after 3rd irrigation) and 9h (after 5th irrigation). The σ_a values are relatively low, mostly ranging from 5 to 35 mS m^{-1}. Note that σ_a series tend to remain approximately in the initial range in the non-irrigated half transect. For the remaining half transect, a similar spatial pattern is observed in both VCP and HCP configurations, with values progressively higher from ρ32 to ρ118, which is coherent with the presence of the water table at relatively low depth. For the same receiver spacings, the HCP configuration shows higher σ_a values than the VCP configuration, which indicate the presence of a conductive zone at shallower depths, and is consistent with the propagation of a wetting front increasing soil conductivity as water infiltrates into the soil profile.

https://doi.org/10.5194/egusphere-2026-1414
Preprint. Discussion started: 4 May 2026

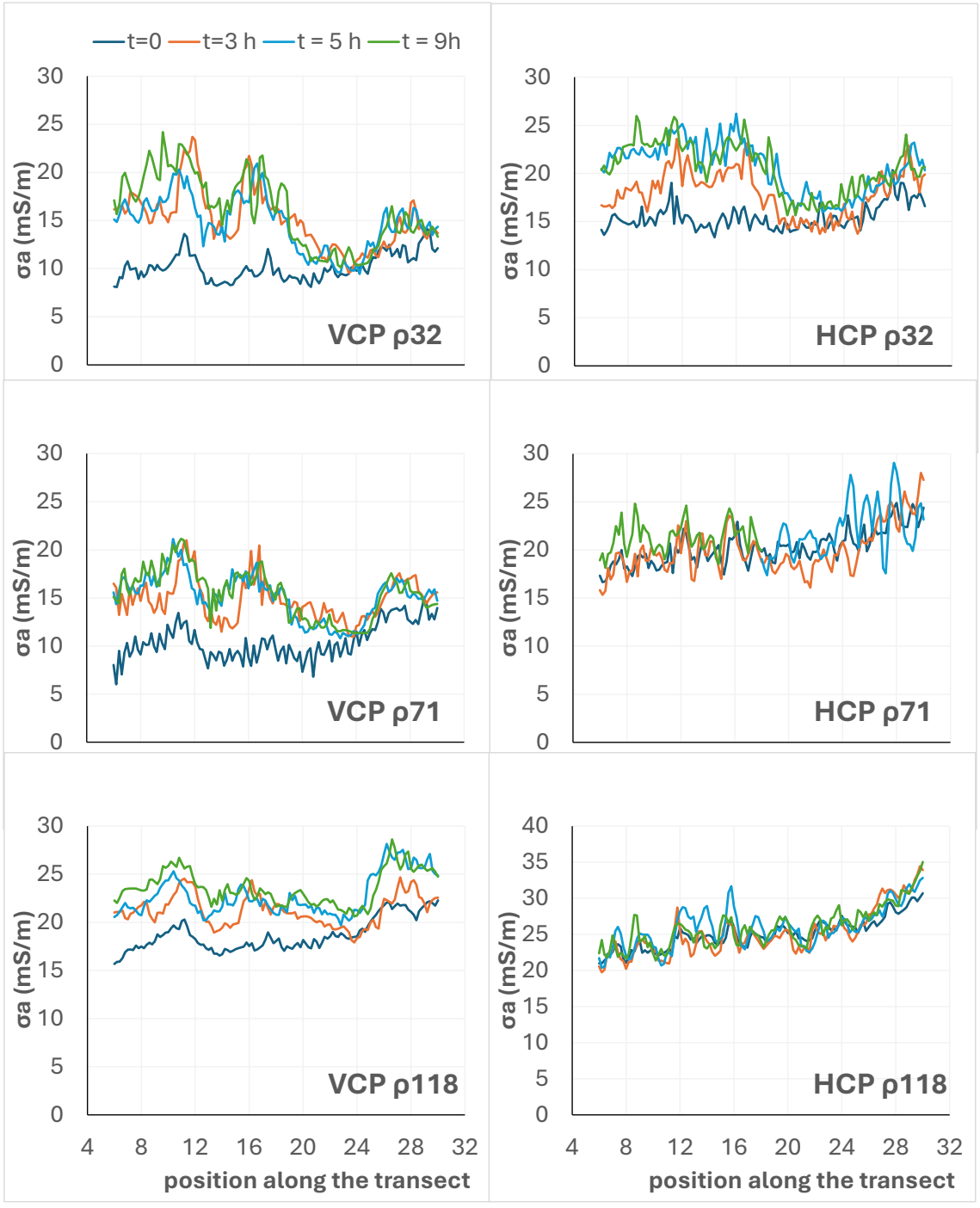

Figure 3: spatial distribution of the EMI σ_a under the VCP configuration and HCP configuration for the three receiver coil spacings (ρ32, ρ71, and ρ118) measured at the beginning (t=0) and during the water infiltration experiment after the 3h (after 2nd irrigation), 5h (after 3rd irrigation) and 9h (after 5th irrigation)

https://doi.org/10.5194/egusphere-2026-1414
Preprint. Discussion started: 4 May 2026

In terms of temporal variability, σ_a values clearly increase in both VCP and HCP configurations during the first five hours of the experiment. After this period, σ_a values remain relatively stable until the end of the experiment.

In the inversion of the σ_a data, the regularization parameter λ was optimized, as described in Section 2.4. Results from several tests (not shown here) suggested that λ values between 1 and 5 provide the best performance for resolving the spatiotemporal distribution of σ_b in the context of the infiltration experiment under study.

Figure 4 shows the σ_b distributions coming from the time-lapse inversion of the σ_a data presented in figure 3. The model can predict the propagation of a wetting front in the irrigated half of the transect, as indicated by the gradual formation and deepening of a more conductive zone within the soil profile after irrigation begins, in agreement with the information provided by the σ_a measurements. Beneath this conductive layer, a resistive zone is evident where σ_b values remain around 20 mS m^{-1}. At the bottom, a soil layer with relatively higher conductivity (about 30 mS m^{-1}) appears, resulting from the assignment of higher conductivity in the inversion to account for the presence of a water table at approximately 120–130 cm.

Note that the model is also able to predict a temporally stable σ_b pattern in the non-irrigated half transect, which was considered as an indirect way to check the reliability of the inversion strategy.

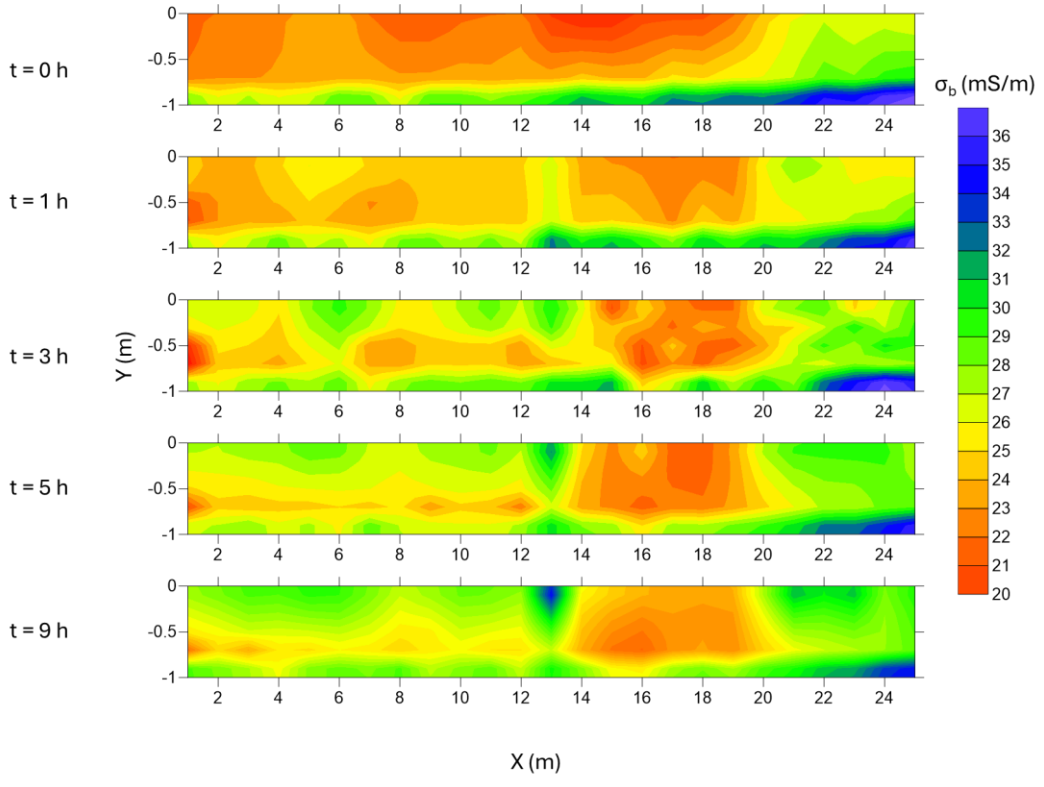

Figure 4: σ_b distributions coming from the time-lapse inversion of the σ_a data presented in figure 3. Four times from the start of irrigation were selected (t = 0, 1, 3, 5 and 9 h), where the propagation of the wetting front is clearly evident.

https://doi.org/10.5194/egusphere-2026-1414
Preprint. Discussion started: 4 May 2026

3.2 Converting σ_b to θ distributions

Figure 5 shows the soil-specific σ_b-θ calibration obtained by the TDR readings, as described in the section 2.2. Building of the site-specific ρ_b-θ relationship. A clear linear relationship was found, has expected in a soil characterized by an initially low and relatively constant salinity. The graph also reports the corresponding coefficients of the linear relationship, together with the coefficients of determination, R^2.

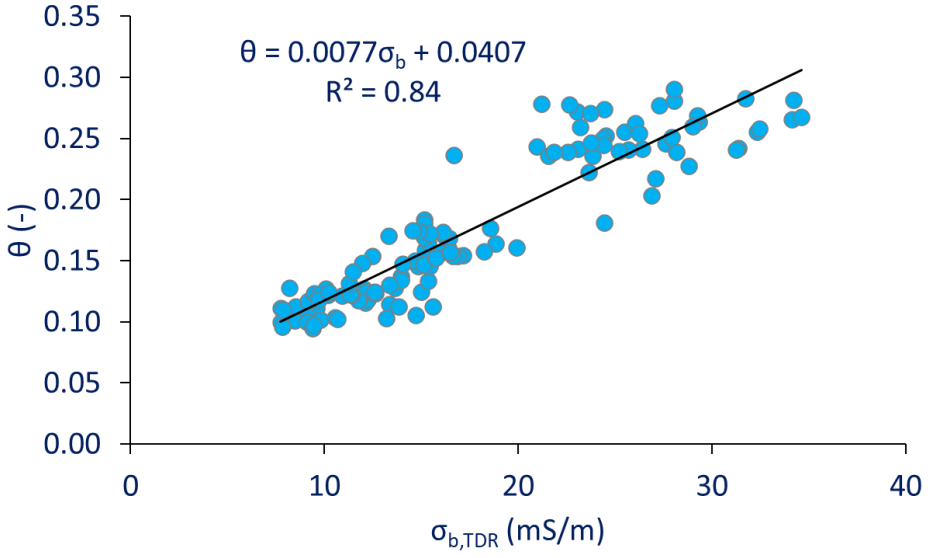

Figure 5: The σ_b-θ relationship obtained by TDR measurements carried out in the surface soil layer during the transect infiltration experiment. The label $\sigma_{b,TDR}$ has been used to avoid confusions with the σ_b coming from the EMI inversion.

Figure 6 shows the distributions of θ coming from the conversion of the EMI estimations of σ_b, based on the site-specific σ_b-θ relationship. Again, only three times from the start of irrigation were selected, where the propagation of the wetting front is clearly evident. The maps refer only to the irrigated half transect. For the sake of comparison, the figure also reports the θ distributions obtained by the auger sampling.

https://doi.org/10.5194/egusphere-2026-1414
Preprint. Discussion started: 4 May 2026

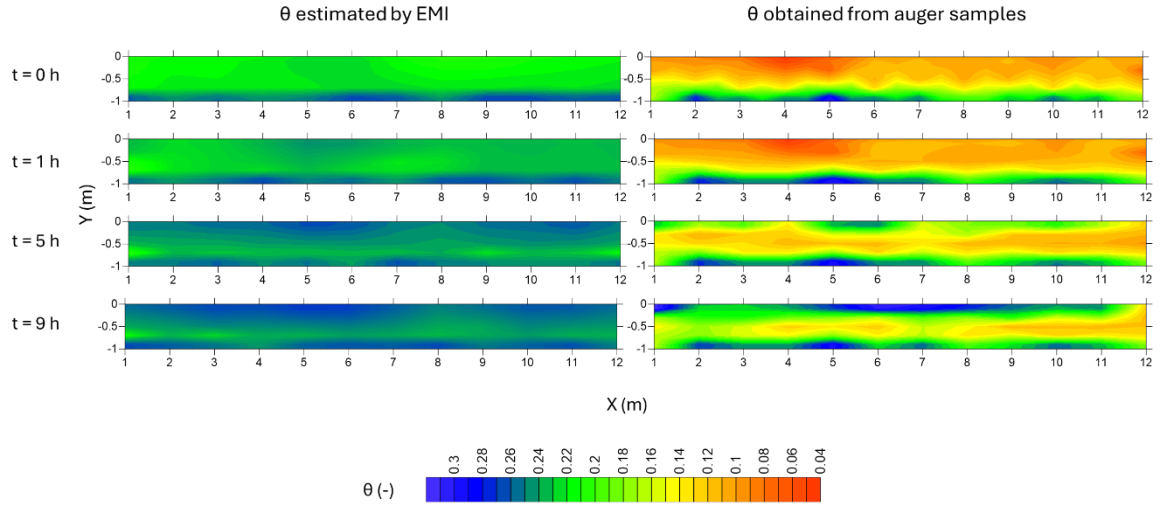

Figure 6: Left panel: θ distributions obtained from the conversion of the EMI estimations of σ_b, based on the site-specific σ_b-θ relationship; Right panel: θ distributions obtained by the auger sampling. Only three times from the start of irrigation were selected, where the propagation of the wetting front is clearly evident. The maps refer only to the irrigated half transect.

Both maps clearly show a gradual propagation of the wetting front during the irrigation experiment. However, it is immediately evident that the EMI-based estimates indicate relatively uniform water contents within a limited range (0.17–0.27), overlooking the lower water contents (the red layers in the auger maps). This behaviour confirms what has been frequently found in the literature. Compared to point-scale measurements, EMI sensors average out local-scale variations in water content due to their larger observation volume and signal processing. As a result, EMI sensors effectively capture broader spatial and temporal trends in soil water content, whereas auger sampling is more sensitive to localized changes and short-term fluctuations, producing more variable but precise measurements at specific points. This, combined with the smoothness constraint applied in the inversion process to stabilize the solution, also limits the ability to resolve sharp water content variations observed in the auger-based measurements. In other words, auger samples capture the infiltration process in detail, including high-frequency effects from local heterogeneities that influence the horizontal fluctuation of the wetting front. In contrast, EMI measurements spatially smooth these small-scale effects and describes the macroscopic behaviour of the process across the entire transect. To an extent, it might be deduced that EMI measurements observe the same infiltration process as the auger samples but at a coarser support scale. Trying to scale empirically the two water content distributions at different time would be cumbersome, as it would require complex time- and depth-dependent corrections due to the varying sensitivity (and response) of the EMI sensor with the varying position of the wetting front. It would also hide the physical basis behind this behaviour.

As suggested by the results in Dragonetti et al. (2022), EMI- and auger sampling-based processes could be interpreted as two scaled representations of the same infiltration process, which could thus be reconciled within a physically based Richards-equation framework, by appropriately scaling the hydraulic parameters and initial conditions, to align the macroscopic

https://doi.org/10.5194/egusphere-2026-1414
Preprint. Discussion started: 4 May 2026

behaviour observed by EMI to that deduced from auger observations. This approach would provide a relatively simple, physically based, scaling methodology that explicitly accounts for the intrinsic nonlinearity of both the infiltration process and the EMI response. In other words, this implies scaling the whole infiltration process rather than attempt to empirically rescale individual measurements.

The graphs in the Figure 7 show six of the twelve θ profiles observed by auger sampling and simulated by FLOWS with the SHP measured in the two soil horizons by infiltrometer and reported in table 2. The profiles refer to three different times (1h, 5h and 9h) from the beginning of the infiltration experiment infiltration experiment. As already mentioned in the Materials and Methods section, we assumed that the SHPs determined from infiltrometer measurements of the two identified soil horizons are representative for all 1D soil profiles along the transect, thus neglecting any SHP spatial variability. By contrast, the initial conditions were set to the measured water contents at various depths for each auger data profile, while the top boundary conditions were defined by the irrigation rates actually measured using the rain sampler cylinders during the irrigation applications. The Root-Mean-Square Error, RMSE, between the auger-measured and the simulated water contents, was calculated for each site. A generally good agreement between measurements and simulations can be observed, with RMSE ranging between 0.025 and 0.053, even considering that the simulations were performed without any adjustment of the soil hydraulic parameters and that a single set of SHPs was used to describe infiltration behaviour along the entire transect. It is also important to note potential uncertainties in the water content measurements, arising from difficulties in accurately sampling the correct depth intervals with the auger and from partial collapse of soil at shallower depths during sampling.

https://doi.org/10.5194/egusphere-2026-1414
Preprint. Discussion started: 4 May 2026

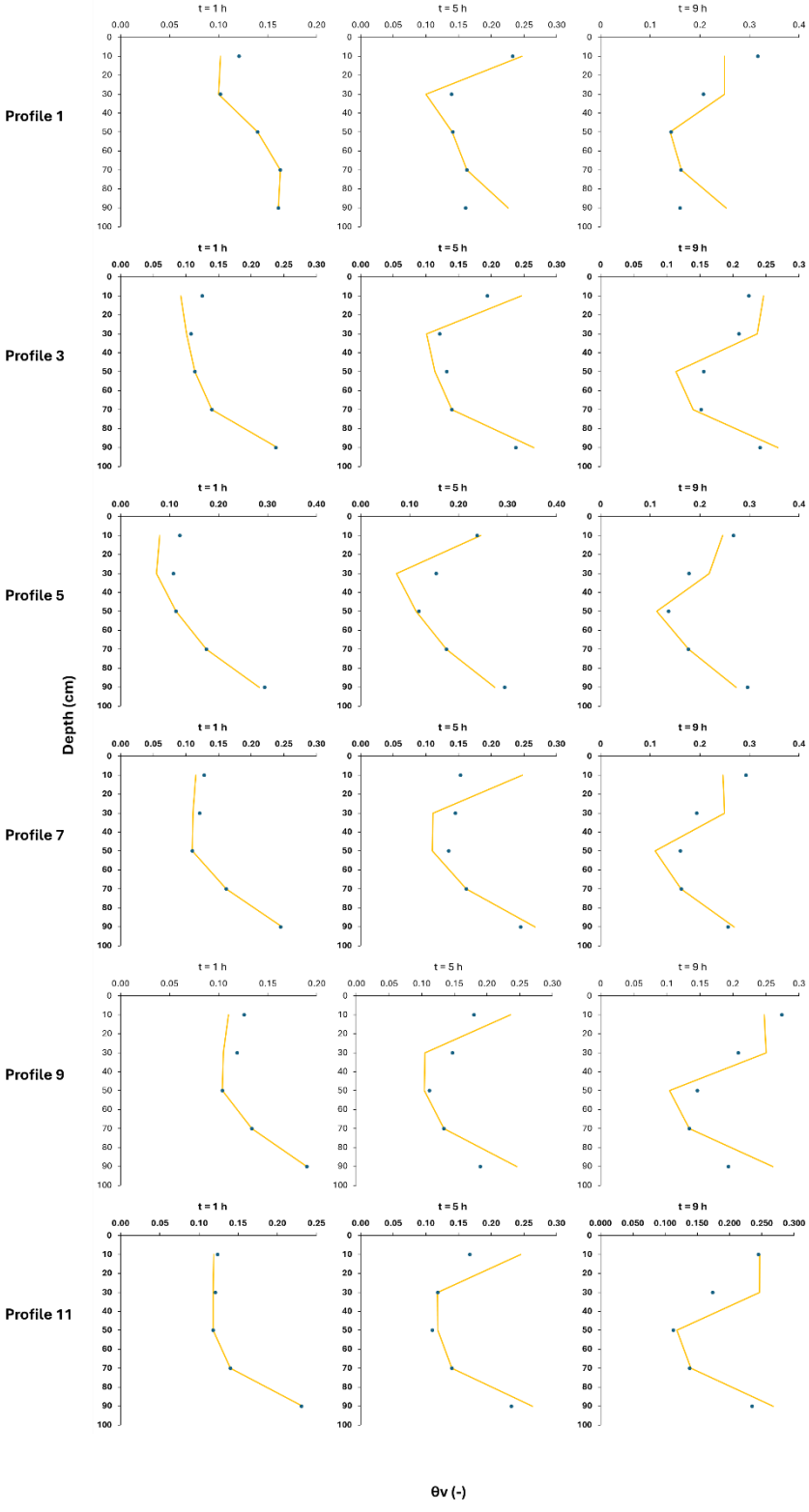

https://doi.org/10.5194/egusphere-2026-1414
Preprint. Discussion started: 4 May 2026

Figure 7: Six of the twelve θ profiles observed by auger sampling (symbols) and simulated by FLOWS (lines) with the SHP measured in the two soil horizons by infiltrometer and reported in table 2. The profiles refer to three different times (1h, 5h and 9h) from the beginning of the infiltration experiment.

485 The good agreement between measurements and FLOWS simulations along the whole transect may be deduced by observing the corresponding θ maps obtained at four different times during the infiltration experiment (see Figure 8). Note how the simulated distributions closely match the measured ones, providing essentially the same description of wetting front propagation observed in the measurements. These results indicate that the model can be regarded as a reliable tool for continuously describing the infiltration process represented by the discrete direct observations.

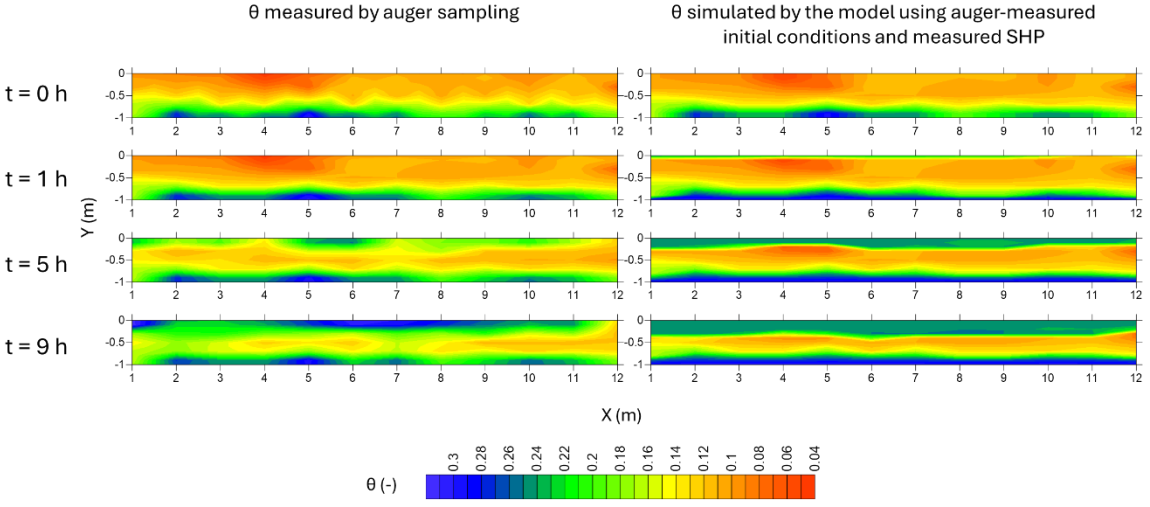

Figure 8: Left panel: θ distributions obtained by the auger sampling; Right panel: θ distributions simulated by FLOWS. Only three times from the start of irrigation were selected, where the propagation of the wetting front is clearly evident. The maps refer only to the irrigated half transect. The scale in for θ values.

490 Following the suggestions by Dragonetti et al. (2022), we tried to simulate the θ profiles estimated by the EMI by adopting for each of the twelve profiles the corresponding estimated water content values provided by the EMI readings at t = 0. The boundary conditions were again set at the rainfall rate applied by irrigation in the different parts of the transect. The SHP were adjusted by simply reducing the saturated water content by a factor varying in the range 0.7-0.9. To identify the value of that factor, three values were used, 0.7, 0.8 and 0.9, and the value 0.8 was found to be the most suitable choice as it led to simulated
495 water contents close to those estimated by EMI, as shown in figure 9. Thus, the scaling factor value was selected empirically. It is worth noting that the choice of this scaling factor is the only empirical step of the whole procedure, which remains mostly physically based.

Figure 9 shows six of the twelve EMI-based θ profiles alongside the corresponding simulations obtained with FLOWS under the conditions described above, using a scaling factor of 0.8 for the saturated water content in both horizons. The simulated θ
500 distributions reproduce quite satisfactorily the measured profiles, providing a very similar representation of the wetting front

https://doi.org/10.5194/egusphere-2026-1414
Preprint. Discussion started: 4 May 2026

propagation. The graphs corresponding to site 1 include also the simulated water contents using reduction factors of 0.7 and 0.9 for the saturated water content. The graphs corresponding to site 1 demonstrate the reasoning behind selecting the reduction factor value of 0.8. This value was found to give similarly satisfying results, in terms of simulated water contents, for the other profiles as well. However, we opted to show those results for site 1 only to maximize the visibility of the figure.

The θ maps in Figure 10 confirm the agreement between EMI estimations and FLOWS simulations along the whole transect. From both the profiles and the maps, only at 9 hours the model predicts some thin layer of water accumulation at around 50 cm depth, which is smoothed out by EMI for the reasons already discussed.

The RMSE between the EMI-based and the simulated water contents was calculated for each site. Overall, as expected, the model reproduces the EMI-estimated θ patterns quite accurately, with RMSE ranging between 0.013 and 0.018, implicitly suggesting that EMI actually observes at the same infiltration process as that described by point-scale measurements but confined in a narrower water content range and starting from a different initial condition.

https://doi.org/10.5194/egusphere-2026-1414
Preprint. Discussion started: 4 May 2026

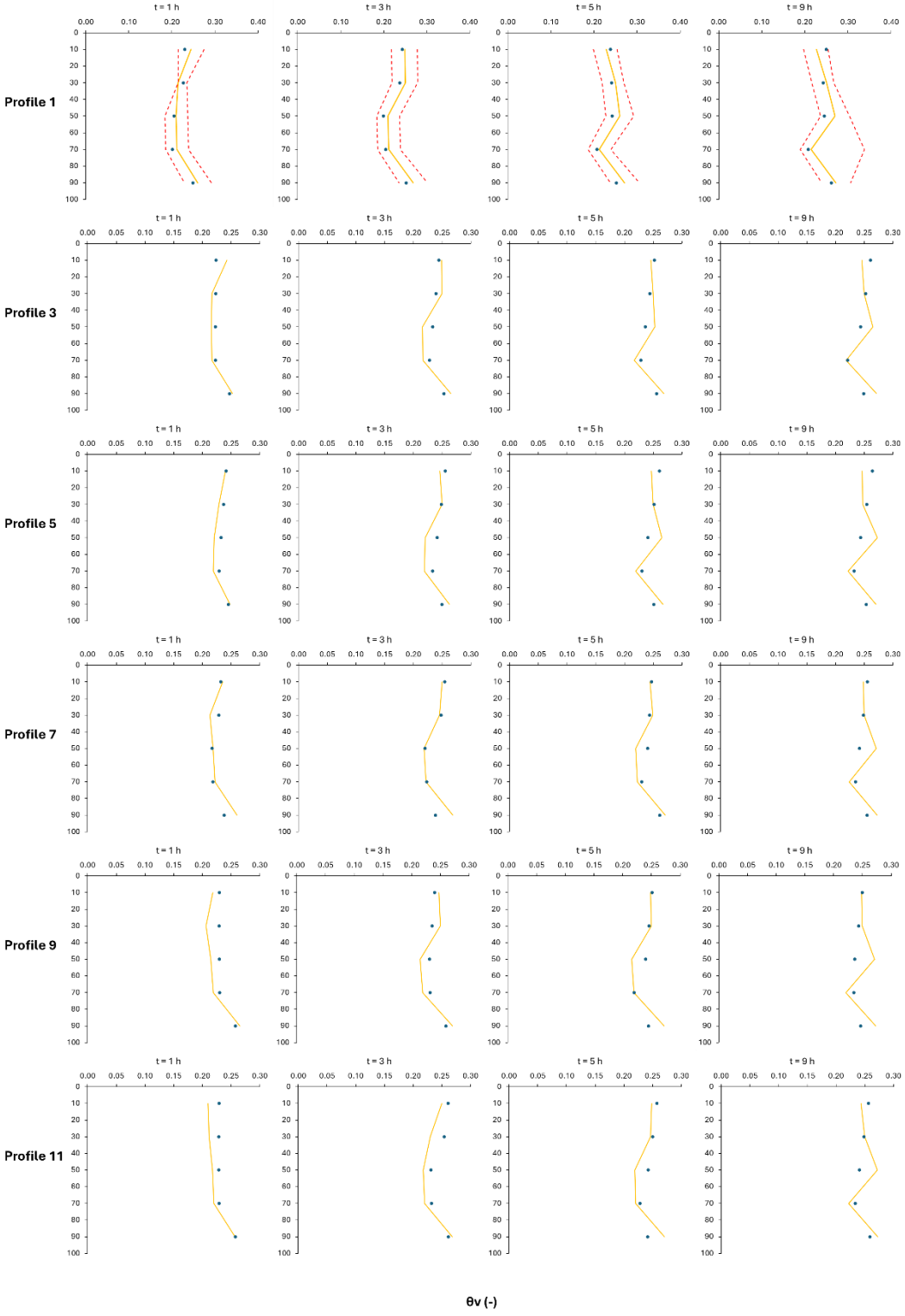

https://doi.org/10.5194/egusphere-2026-1414
Preprint. Discussion started: 4 May 2026

Figure 9: Six of the twelve θ profiles estimated by EMI (symbols) and simulated by FLOWS (lines) with the SHPs scaled using a reduction factor of 0.8 for the saturated water content and with initial conditions for each profile set to the water content values estimated by the EMI at t = 0. The profiles refer to four different times (1h, 3h, 5h and 9h) from the beginning of the infiltration experiment.

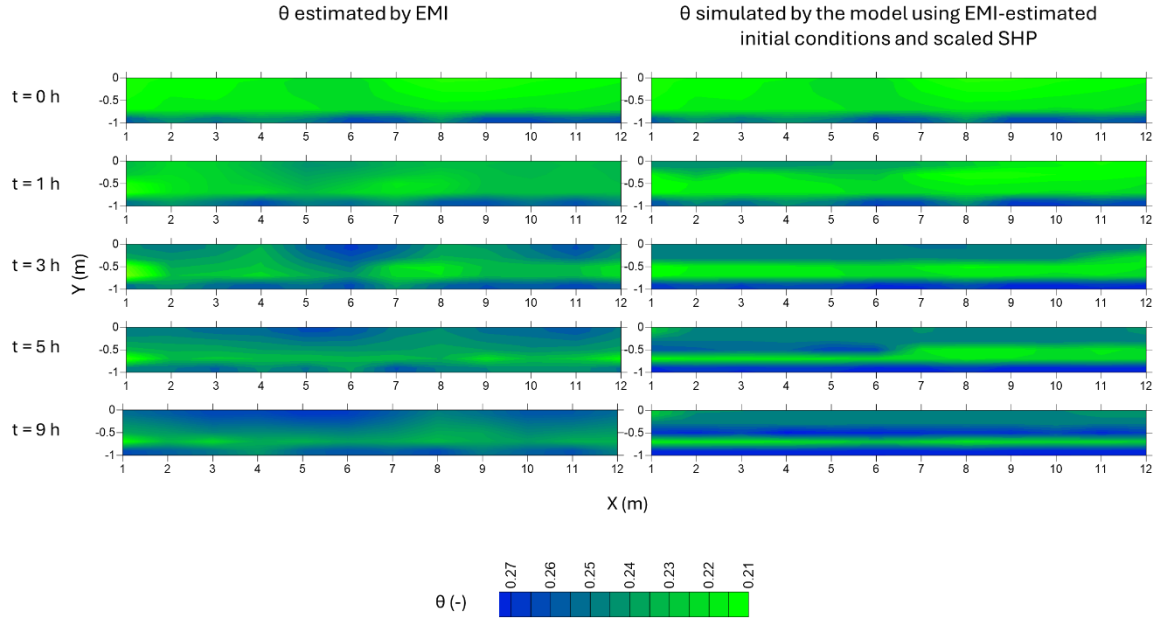

Figure 10: Left panel: θ distributions estimated by EMI; Right panel: θ distributions simulated by FLOWS. The maps refer only to the irrigated half transect

The hydrological model can therefore be used as a physically based interpretative tool to understand what an EMI sensor observes. In this context, simply scaling the SHP and assigning the initial conditions consistent with the EMI observations effectively provide the conversion tool needed to relate the two representations of the process; through the hydrological model, this scaling allows the conversion between the high-frequency, microscopic description obtained from auger sampling or other point-scale measurements and the low-frequency, macroscopic description provided by EMI measurements of the same infiltration process. This way, the differences in the θ distributions, which change nonlinearly over time as the wetting front propagates, are automatically reconciled without the need for empirical scaling.

This is clearly confirmed in the Figure 11. The left panel in figure shows the maps of the θ distributions simulated by using the original SHP and the auger-based initial conditions. Similarly, the maps in the right panel of the figure were obtained by simulations with the same SHPs and by scaling the initial water content conditions estimated by EMI to match those obtained from auger measurements. This was achieved by multiplying the EMI-estimated initial conditions by a depth-dependent scaling factor, ensuring that at each depth, the average EMI-estimated water content was equal to the corresponding average measured by the auger. The high similarity of the two simulations clearly demonstrates that simulations based on EMI-scaled initial

https://doi.org/10.5194/egusphere-2026-1414
Preprint. Discussion started: 4 May 2026

conditions and SHPs can effectively be used to reproduce what one would have seen by monitoring the same process through point-scale measurements.

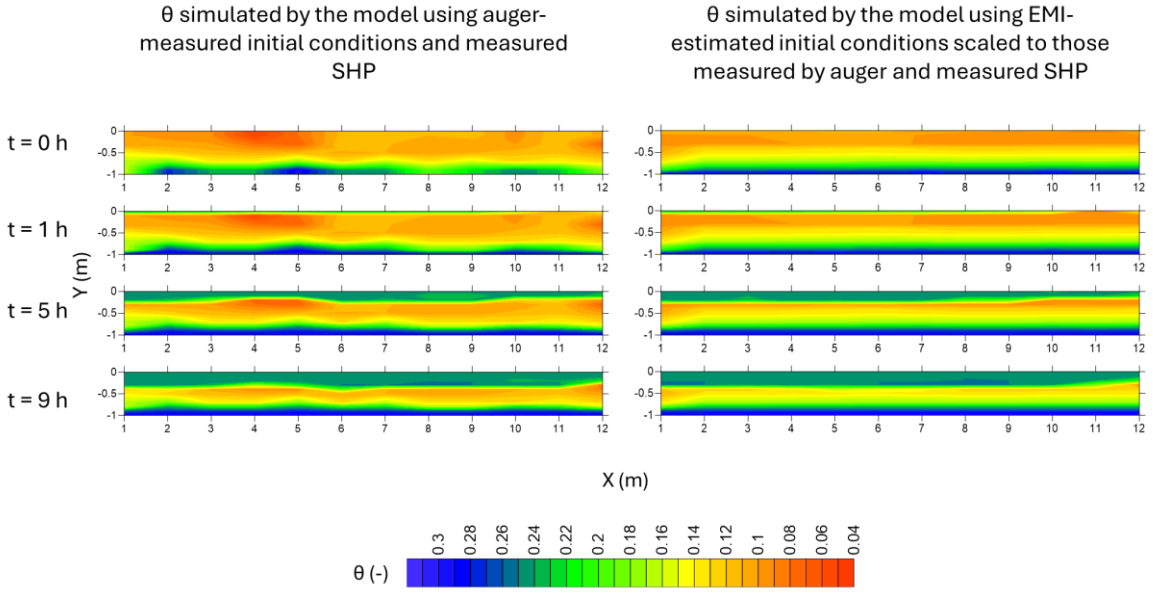

Figure 11: Left panel: maps of the θ distributions simulated by FLOWS using the original SHPs and the auger-based initial conditions; Right panel: θ distributions simulated by FLOWS with the same SHPs and by scaling the initial water content conditions estimated by EMI to match those obtained from auger measurements. Only three times from the start of irrigation were selected, where the propagation of the wetting front is clearly evident. The maps refer only to the irrigated half transect

4 Conclusions

In general, the results of this paper strengthen and extend the results anticipated by Dragonetti et al. (2022). The paper emphasizes the potential of integrating EMI measurements with hydrological modelling in providing a robust physically based framework for interpreting what an EMI sensor observes during a water infiltration experiment, as well as to estimate soil hydraulic properties noninvasively at the field scale.

A relationship between σ_b and θ was built, allowing to estimate the spatio-temporal distribution of the water contents from EMI readings, following an inversion procedure, in an infiltration experiment. This relationship, however, was developed in a sandy soil with negligible clay content and salinity. Nevertheless, the findings of the paper have very relevant practical implications for using the EMI for soil hydraulic characterizations. The proposed method demonstrates that the EMI sensor observes SHP similar to those obtained using point-scale measurements, e.g., by auger samples, with the only difference is that EMI observes θ_s reduced by a factor of 0.8.

https://doi.org/10.5194/egusphere-2026-1414
Preprint. Discussion started: 4 May 2026

In practice, a short infiltration experiment can be monitored at high temporal resolution using an EMI sensor, and the resulting water content estimates can be used in an inversion procedure to determine EMI-based SHPs. Contextually, an initial soil water content profile could be also obtained by direct sampling or by point-scale probes. These well-defined initial conditions, which capture high-frequency variations due to local heterogeneities, can then be used to scale the smoothed initial conditions detected by the EMI. Additionally, the saturated water content of the different soil horizons should be known, allowing the EMI-based soil hydraulic properties to be scaled to match those that would be obtained from local-scale measurements of the same infiltration process. The scaled SHPs and initial conditions could thus be used to reproduce what one would have seen by monitoring the same process through point-scale measurements.

Importantly, the proposed methodology does not require prior calibration of EMI readings due to unknown shift and large observation volume, as these effects are implicitly incorporated into the EMI-based derived water content distributions and in the SHPs coming from hydraulic inversion of these water contents. Only after the completion of the entire procedure, these EMI-based SHPs, which are able to describe the infiltration process at a macroscopic scale, may be appropriately scaled to provide all the sharp water content changes which would be detected by local scale sensors.

Code, data, or code and data availability

Details on FLOWS model theory, user interface and numerical solutions are provided in Coppola et al. (2025). Data utilized in this study can be available upon request. We are unable to publish the complete datasets collected for this study, as they will be included in a forthcoming follow-up paper, where all datasets will be made publicly available.

Author contributions

AC. Conceptualization, Formal analysis, Funding acquisition, Investigation, Methodology, Software, Supervision, Visualization, Writing (original draft preparation), Writing (review and editing). AV. Data curation, Funding acquisition, Investigation, Resources, Validation, Writing (Review and editing). GPD. Formal analysis, Funding acquisition, Investigation, Methodology, Resources, Validation, Visualization, Writing (original draft preparation), Writing (review and editing). FL. Investigation, Writing (review and editing). SDP. Investigation, Writing (review and editing). FS. Investigation, Data curation, Writing (review and editing). SBMH. Formal analysis, Investigation, Methodology, Visualization, Writing (original draft preparation), Writing (review and editing)

Competing interests

The corresponding author declares that none of the authors has any competing interests.

https://doi.org/10.5194/egusphere-2026-1414
Preprint. Discussion started: 4 May 2026

Disclaimer

Copernicus Publications adds a standard disclaimer: "Copernicus Publications remains neutral with regard to jurisdictional claims made in the text, published maps, institutional affiliations, or any other geographical representation in this paper. While Copernicus Publications makes every effort to include appropriate place names, the final responsibility lies with the authors. Views expressed in the text are those of the authors and do not necessarily reflect the views of the publisher."
Please feel free to add disclaimer text at your choice, if applicable.

Acknowledgements

This work was supported by the PRIN 2022 project entitled "Monitoring and modelling of contaminants transport in soil across spatial scales", funded by the Italian Ministry of University and Research (MUR) – Prot. 20229FCFMM – CUP C53D23005140006

Financial support

This study was carried out within the PRIN project "Monitoring and modelling of contaminants transport in soil across spatial scales" and received funding from the Italian Ministry of University and Research (MUR) – Prot. 20229FCFMM – CUP C53D23005140006

Review statement

The review statement will be added by Copernicus Publications listing the handling editor as well as all contributing referees according to their status anonymous or identified.

References

Altdorff, D., Galagedara, L., Nadeem, M., Cheema, M., and Unc, A.: Effect of agronomic treatments on the accuracy of soil moisture mapping by electromagnetic induction, Catena (Amst), 164, 96–106, https://doi.org/10.1016/j.catena.2017.12.036, 2018

Amezketa, E.: An integrated methodology for assessing soil salinization, a pre-condition for land desertification, J. Arid Environ., 67, 594–606, https://doi.org/10.1016/j.jaridenv.2006.03.010, 2006.

https://doi.org/10.5194/egusphere-2026-1414
Preprint. Discussion started: 4 May 2026

Ankeny, M.D., Kaspar, T.C., Horton, R.: Design for an Automated Tension Infiltrometer. Soil Sci. Soc. Am. J. 52(3), 893–896. John Wiley & Sons, Ltd. doi: https://doi.org/10.2136/sssaj1988.03615995005200030054x, 1988

Autovino D., A. Coppola, R. De Mascellis, M. Farzamian and A. Basile: An in-situ methodology to separate the contribution of soil water content and salinity to EMI-based soil electrical conductivity. SOIL, 12, 37–54, 2026. https://doi.org/10.5194/soil-12-37-2026, 2026

Badewa, E., Unc, A., Cheema, M., Kavanagh, V., and Galagedara, L.: Soil moisture mapping using multi-frequency and multi-coil electromagnetic induction sensors on managed podzols, Agronomy, 8, https://doi.org/10.3390/agronomy8100224, 2018.

Basile A., Ciollaro G., Coppola A.: Hysteresis in soil-water characteristics as a key to interpreting comparisons of laboratory and field measured hydraulic properties. Water Resour. Res., 39(12), 1355, doi:10.1029/2003WR002432, 2003

Basile A., Coppola A.: Preface to the Special Issue "Soil Hydrology in Agriculture". Water 2019, 11, 1430; doi:10.3390/w11071430, 2019

Basile A., Coppola A., De Mascellis R., Randazzo L.: A hysteresis based scaling approach to deduce field hydraulic behaviour from core scale measurements. Vadose Zone Journal, 5:1005–1016 (2006), doi:10.2136/vzj2005.0128, 2006

Brevik, E. C., Fenton, T. E., and Lazari, A.: Soil electrical conductivity as a function of soil water content and implications for soil mapping, Precis. Agric., 7, 393–404, https://doi.org/10.1007/s11119-006-9021-x, 2006.

Camporese, M., Cassiani, G., Deiana, R., Salandin, P., and Binley, A.: Coupled and uncoupled hydrogeophysical inversions using ensemble Kalman filter assimilation of ERT monitored tracer test data, Water Resour. Res., 51, 3277–3291, https://doi.org/10.1002/2014WR016017, 2015.

Comegna A., Coppola A., Comegna V., Severino G., Sommella A., Vitale C.: State-space approach to evaluate spatial variability of field measured soil water status along a line transect in a volcanic-vesuvian soil. Hydrol. Earth Syst. Sci., 14, 2455–2463, 2010. doi:10.5194/hess-14-2455-2010, 2010

Comegna, A., Dragonetti, G., Kodesova, R., Coppola A.: Impact of olive mill wastewater (OMW) on the soil hydraulic and solute transport properties. Int. J. Environ. Sci. Technol. (2021). https://doi.org/10.1007/s13762-021-03630-6, 2021

Comegna, A.; Hassan, S.B.M.; Coppola, A.: Development and Application of an IoT-Based System for Soil Water Status Monitoring in a Soil Profile. Sensors 2024, 24, 2725. https://doi.org/10.3390/s24092725, 2024

https://doi.org/10.5194/egusphere-2026-1414
Preprint. Discussion started: 4 May 2026

Cook, P.G. & Walker, G.R.:. Depth profiles of electrical conductivity from linear combinations of electromagnetic induction measurements. Soil Science Society of America Journal, 56, 1015–1022, 1992

Coppola A., A. Basile, M. Menenti, M. Buonanno, J. Colin, R. De Mascellis, M. Esposito, U. Lazzaro, V. Magliulo, P. Manna: Spatial distribution and structure of remotely sensed surface water content estimated by a thermal inertia approach. Remote Sensing for Environmental Monitoring and Change Detection (Proceedings of Symposium HS3007 at IUGG2007, Perugia, July 2007). IAHS Publ. 316, 2007

Coppola A., Basile A., Comegna A., Fenu C., Concas A., Pili F., Hassan S. B. M.: FLOWS: A model to simulate water and solutes fluxes in agricultural and environmental systems. 1. Theory and applications with intercode benchmarking. Engineering with computers. Springer Nature. In press, 2026a

Coppola A., Basile A., Comegna A., Fenu C., Concas A., Pili F., Hassan S. B. M.: FLOWS: A model to simulate water and solutes fluxes in agricultural and environmental systems. 2. Modules for specific applications in agro-hydrological modeling. Engineering with computers. Springer Nature. In press, 2026b

Coppola A., Dragonetti G., Sengouga A., Lamaddalena N., Comegna A., Basile A., Noviello N. and Nardella L: Identifying Optimal Irrigation Water Needs at District Scale by Using a Physically Based Agro-Hydrological Model. Water. doi: 10.3390/w11040841, 2019

Coppola A., Hassan S. and Pili F.: FLOWS - FLOw of Water and Solutes in agricultural and environmental systems. Zenodo. doi: https://doi.org/10.5281/zenodo.17076523, 2025

Coppola A., K. Smettem, A. Ajeel, A. Saeed, G. Dragonetti, A. Comegna, N. Lamaddalena, A. Vacca: Calibration of an electromagnetic induction sensor with time-domain reflectometry data to monitor root zone electrical conductivity under saline water irrigation. European Journal of Soil Science, 67, 737–748. doi: 10.1111/ejss.12390, 2016

Coppola A., Zucaro R., Baralla S., Satta M., Ruberto M., Comegna A., Dragonetti G. and Hassan S.B.M.: Monitoring and Modelling Fluxes of Water and Nutrients to Surface Drainage Network From Irrigated Agricultural Fields in a Hydraulically Reclaimed Coastal Area. Ecohydrology, 17(8): e2723. John Wiley & Sons, Ltd. doi: https://doi.org/10.1002/eco.2723, 2024

Corwin, D.L. & Rhoades, J.D.: Measurement of inverted electrical conductivity profiles using electromagnetic induction. Soil Science Society of America Journal, 48, 288–291, 1984

Deidda, G. P., Bonomi, E., and Manzi, C.: Inversion of electrical conductivity data with Tikhonov regularization approach: some considerations, Ann. Geophys., 46, 549–558, 2003.

https://doi.org/10.5194/egusphere-2026-1414
Preprint. Discussion started: 4 May 2026

Deidda, G. P., Fenu, C., and Rodriguez, G.: Regularized solution of a nonlinear problem in electromagnetic sounding, Inverse Probl., 30, 125014, https://doi.org/10.1088/0266-5611/30/12/125014, 2014.

Deidda, G.P., Díaz de Alba, P., Pes, F., Rodriguez, G.: Forward Electromagnetic Induction Modelling in a Multilayered Half-Space: An Open-Source Software Tool. Remote Sens., 15, 1772, doi.org/10.3390/rs15071772, 2023

Deidda, G.P., Díaz de Alba, P., Rodriguez, G., Vignoli, G.: Inversion of Multiconfiguration Complex EMI Data with Minimum Gradient Support Regularization: A Case Study. Math. Geosci., 52, 945–970, doi:10.1007/s11004-020-09855-4, 2020

Díaz de Alba, P. and Rodriguez, G.: Regularized Inversion of Multi-Frequency EM Data in Geophysical Applications, in: Trends in Differential Equations and Applications, SEMA SIMAI Springer Series, vol. 8, edited by: Ortegón Gallego, F., Redondo Neble, M., and Rodríguez Galván, J., Springer, Cham, https://doi.org/10.1007/978-3-319-32013-7_20, 2016.

Dragonetti, G., Comegna A., Ajeel A., Deidda G.P., Lamaddalena N., Rodriguez G., Vignoli G., Coppola A: Calibrating electromagnetic induction conductivities with time-domain reflectometry measurements. Hydrol. Earth Syst. Sci., 22, 1509–1523, 2018 https://doi.org/10.5194/hess-22-1509-2018, 2018

Dragonetti, G., Farzamian, M., Basile, A., Monteiro Santos, F., and Coppola, A.: In situ estimation of soil hydraulic and hydrodispersive properties by inversion of electromagnetic induction measurements and soil hydrological modeling, Hydrol. Earth Syst. Sci., 26, 5119–5136, https://doi.org/10.5194/hess-26-5119-2022, 2022.

Farzamian M., Autovino D., Basile A., De Mascellis R., Dragonetti G., Monteiro Santos F., Binley A., Coppola A.: Assessing the dynamics of soil salinity with time-lapse inversion of electromagnetic data guided by hydrological modelling. Hydrol. Earth Syst. Sci., 25, 1509–1527, 2021. https://doi.org/10.5194/hess-25-1509-2021, 2021

Fusco F., Allocca V., Bancheri M., Basile A., Calcaterra D., Coppola A., Neuwirth M., Puig-Sirera À., Terribile F. and De Vita P.: A multi-method approach for assessing groundwater vulnerability of shallow aquifers in the Marchfeld region (Austria). Journal of Hydrology: Regional Studies, 54: 101865. doi: https://doi.org/10.1016/j.ejrh.2024.101865, 2024

Hassan, S.B.M., Dragonetti, G., Comegna, A., Lamaddalena N., Coppola A: Analyzing the role of soil and vegetation spatial variability in modelling hydrological processes for irrigation optimization at large scale. Irrig Sci (2024). https://doi.org/10.1007/s00271-023-00882-7, 2025

Hassan, S.B.M., Dragonetti, G., Comegna, A., Sengouga, A., Lamaddalena, N., Coppola, A.: A Bimodal Extension of the ARYA&PARIS Approach for Predicting Hydraulic Properties of Structured Soils, Journal of Hydrology (2022), doi: https://doi.org/10.1016/j.jhydrol.2022.127980, 2022

https://doi.org/10.5194/egusphere-2026-1414
Preprint. Discussion started: 4 May 2026

Hedley, C.B., Roudier, P., Yule, I.J., Ekanayake, J. & Bradbury, S.: Soil water status and water table depth modelling using electromagnetic surveys for precision irrigation scheduling. Geoderma, 199, 22–29, 2013

Heimovaara, T.J., Focke, A.G., Bouten, W. & Verstraten, J.M.: Assessing temporal variations in soilwater compositionwith time domain reflectometry. Soil Science Society of America Journal, 59, 689–698, 1995

Hendrickx, J.M.H., Borchers, B., Corwin, D.L., Lesch, S.M., Hilgendorf, A.C. & Schlue, J.: Inversion of soil conductivity profiles from electromagnetic induction measurements: theory and experimental verification. Soil Science Society of America Journal, 66, 673–685, 2002

Hinnell, A. C., Ferre, T. P. A., Vrugt, J. A., Huisman, J. A., Moysey, S., Rings, J., and Kowalsky, M. B.: Improved extraction of hydrologic information from geophysical data through coupled hydrogeophysical inversion, Water Resour. Res., 46, W00D40, https://doi.org/10.1029/2008WR007060, 2010.

Huang, J., Monteiro Santos, F. A., and Triantafilis, J.: Mapping soil water dynamics and a moving wetting front by spatiotemporal inversion of electromagnetic induction data, Water Resour. Res., 52, 9131–9145, https://doi.org/10.1002/2016WR019330, 2016

IUSS Working Group WRB.: World Reference Base for Soil Resources. International soil classification system for naming soils and creating legends for soil maps. 4th edition. International Union of Soil Sciences (IUSS), Vienna, Austria, 2022

Kachanoski, R.G., Wesenbeeck, I.V. & Gregorich, E.: Estimating spatial variations of soil water content using noncontacting electromagnetic inductive methods. Canadian Journal of Soil Science, 68, 715–722, 1988

Klotzsche, A., Lärm, L., Vanderborght, J., Cai, G., Morandage, S., Zörner, M., Vereecken, H., and van der Kruk, J.: Monitoring soil water content using timelapse horizontal borehole GPR data at the field-plot scale. Vadose Zone J. 18:190044. doi:10.2136/vzj2019.05.0044, 2019

Lavoué, F., van der Kruk, J., Rings, J., André, F., Moghadas, D., Huisman, J. A., Lambot, S., Weihermüller, L., Vanderborght, J., and Vereecken, H..: Electromagnetic induction calibration using apparent electrical conductivity modelling based on electrical resistivity tomography, Near Surf. Geophys., 8, 553–561, 2010.

Ley-Cooper, A. Y., Viezzoli, A., Guillemoteau, J., Vignoli, G., Macnae, J., Cox, L., and Munday, T.: Airborne electromagnetic modelling options and their consequences in target definition, Explor. Geophys., 46, 74–84, https://doi.org/10.1071/eg14045, 2015.

https://doi.org/10.5194/egusphere-2026-1414
Preprint. Discussion started: 4 May 2026

Monteiro Santos, F. A.: 1-D laterally constrained inversion of EM34 profiling data, J. Appl. Geophy., 56, 123–134, https://doi.org/10.1016/j.jappgeo.2004.04.005, 2004.

Mualem, Y.: A new model for predicting the hydraulic conductivity of unsaturated porous media. Water Resour. Res, 12, 3, 513–522. https://doi.org/10.1029/ WR012i003p00513, 1976

Porru M.C., Hassan S.B.M., Abdelmaqsoud M.S.M., Vacca A., Da Pelo S. and Coppola A.: Using index and physically-based models to evaluate the intrinsic groundwater vulnerability to non-point source pollutants in an agricultural area in Sardinia (Italy). Frontiers in Water, Volume 6-: doi: 10.3389/frwa.2024.1399170, 2024

Rhoades, J.D. & van Schilfgaarde, J.: An electrical conductivity probe for determining soil salinity. Soil Science Society of America Journal, 40, 647–650, 1976

Robinson, D.A., Jones, S.B., Wraith, J.M., Or, D. & Friedman, S.P.: A review of advances in dielectric and electrical conductivity measurement in soils using time domain reflectometry. Vadose Zone Journal, 2, 444–475, 2003

Schaap, M.G. & Bouten, W.: Modeling water retention curves of sandy soils using neural networks. Water Resources Research, 32 (10), 3033-3040. https://doi.org/10.1029/96WR02278

Serrano, J. M., Shahidian, S., and da Silva, J. R. M.: Apparent electrical conductivity in dry versus wet soil conditions in a shallow soil, Precis. Agric., 14, 99–114, https://doi.org/10.1007/s11119-012-9281-6, 2013.

Sheets, K.R. & Hendrickx, J.M.: Noninvasive soil water content measurement using electromagnetic induction. Water Resources Research, 31, 2401–2409, 1995

Sherlock, M.D. & McDonnell, J.J.: A new tool for hillslope hydrologists: spatially distributed groundwater level and soil water content measured using electromagnetic induction. Hydrological Processes, 17, 1965–1977, 2003

Simunek, J., Genuchten, M.T., Sejna, M.: Development and applications of the HYDRUS and STANMOD software packages and related codes. Vadose Zone J. 7 (2), 587–600, 2008

Simůnek, J., van Genuchten, M.T.: Estimating unsaturated soil hydraulic properties from tension disc infiltrometer data by numerical inversion. Water Resour. Res, 32, 9, 2683–2696. https://doi.org/10.1029/96WR01525, 1996

Slavich, P.G. & Petterson, G.H.: Estimating average root zone salinity from electromagnetic induction (EM-38) measurements. Australian Journal of Soil Research, 28, 453–463, 1990.

https://doi.org/10.5194/egusphere-2026-1414
Preprint. Discussion started: 4 May 2026

Stanley, J.N., Lamb, D.W., Falzon, G. & Schneider, D.A.: Apparent electrical conductivity (ECa) as a surrogate for neutron probe counts to measure soil moisture content in heavy clay soils (Vertosols). Soil Research, 52, 373–378, 2014

Topp, G.C., Davis, J.L. & Annan, A.P.: Electromagnetic determination of soil water content: measurements in coaxial transmission lines. Water Resources Research, 16, 574–582, 1980

Triantafilis, J., Laslett, G. M., and McBratney, A. B.: Calibrating an electromagnetic induction instrument to measure salinity in soil under irrigated cotton, Soil Sci. Soc. Am. J., 64, 1009–1017, https://doi.org/10.2136/sssaj2000.6431009x, 2000

Triantafilis, J., Terhune IV, C. H., and Monteiro Santos, F. A.: An inversion approach to generate electromagnetic conductivity images from signal data, Environmental Modelling & Software, 43, 88–95, https://doi.org/10.1016/j.envsoft.2013.01.012, 2013.

van Genuchten, M.T.: A closed-form equation for predicting the hydraulic conductivity of unsaturated soils. Soil Sci. Soc. Am. J. 44, 892–898, 1980

Vereecken, H., A. Schnepf, J.W. Hopmans, M. Javaux, D. Or, T. Roose, et al.: Modeling soil processes: Review, key challenges, and new perspectives. Vadose Zone J. 15(5). doi:10.2136/vzj2015.09.0131), 2016

Vignoli, G., Fiandaca, G., Christiansen, A. V., Kirkegaard, C., and Auken, E.: Sharp spatially constrained inversion with applications to transient electromagnetic data, Geophys. Prospect., 63, 243–255, 2015.

Vignoli, G., Sapia, V., Menghini, A., and Viezzoli, A.: Examples of Improved Inversion of Different Airborne Electromagnetic Datasets Via Sharp Regularization, J. Environ. Eng. Geophys., 22, 51–61, https://doi.org/10.2113/jeeg22.1.51, 2017.

von Hebel, C., Rudolph, S., Mester, A., Huisman, J. A., Kumbhar P., Vereecken, H., and van der Kruk, J.: Three-dimensional imaging of subsurface structural patterns using quantitative large-scale multiconfiguration electromagnetic induction data, Water Resour. Res., 50, 2732–2748, doi:10.1002/2013WR014864, 2014

Wait, J.: Geo-electromagnetism, Academic Press Inc., 1982

Ward, S. H., & Hohmann, G. W.: Electromagnetic Theory for Geophysical Applications. Society of Exploration Geophysicists, 1988

Wraith, J.M., Comfort, S.D.,Woodbury, B.L. & Inskeep,W.P.: A simplified waveform analysis approach for monitoring solute transport using time-domain reflectometry. Soil Science Society of America Journal, 57, 637–642, 1993

https://doi.org/10.5194/egusphere-2026-1414
Preprint. Discussion started: 4 May 2026

Yao, R. and Jingsong, Y.: Quantitative evaluation of soil salinity and its spatial distribution using electromagnetic induction method, Agr. Water Manage., 97, 1961–1970, https://doi.org/10.1016/j.agwat.2010.02.001, 2010.

Zare H, Hajarian M.: Determination of regularization parameter via solving a multi-objective optimization problem Applied Numerical Mathematics 156(9). Applied Numerical Mathematics 156(9). DOI: 10.1016/j.apnum.2020.05.021, 2020

Zhdanov, M. S., Vignoli, G., and Ueda, T.: Sharp boundary inversion in crosswell travel-time tomography, J. Geophys. Eng., 3, 122–134, 2006